Reworked Precambrian metamorphic basement of the Lhasa terrane, southern Tibet: Zircon/Titanite U–Pb geochronology, Hf isotope and Geochemistry

Dong Xin[1, 2], Zhang Zeming[1], Niu Yaoling[2], Tian Zuolin[1], Zhang Liangliang[3]

1. Key Laboratory of Deep-Earth Dynamics of Ministry of Land and Resources, Institute of Geology, Chinese Academy of Geological Sciences, Beijing, 100037, China
2. Department of Earth Sciences, Durham University, Durham, DH1 3LE, UK
3. State Key Laboratory of Geological Processes and Mineral Resources, and Institute of Earth Sciences, China University of Geosciences, Beijing, 100083, China

ABSTRACT

Due to the paucity of exposure, the formation and evolution of the Precambrian basement of the Lhasa terrane remain poorly known. Here we report zircon and titanite *in situ* U–Pb ages, bulk-rock geochemical and zircon Hf isotopic data on the orthogneisses from the Dongjiu area of the southern Lhasa subterrane (SLT), southern Tibet. Geochemical data suggest that the protoliths of the biotite-amphibole gneiss and biotite gneiss are granodiorite and granite, respectively. Inherited magmatic zircon cores from these orthogneisses give protolith crystalline ages of 1520–1506 Ma, whereas the overgrown zircon rims give metamorphic ages of 605–590 Ma. The

Mesoproterozoic granitic rocks have bulk-rock $\varepsilon_{Nd}(t)$ values of -3.6 to +0.1 and zircon core $\varepsilon_{Hf}(t)$ values of -4.5 to +2.6, which give similar T_{DM2} ages of 2.35–2.05 Ga and 2.54–2.10 Ga respectively, suggesting their derivation from partial melting of Paleoproterozoic crustal material. The granitic rocks are also local provenance for the Mesoproterozoic detrital zircons in the Paleozoic strata in the Lhasa terrane. Titanite *in situ* U–Pb ages further indicate that the Dongjiu orthogneiss experienced more recent metamorphism at ~ 26 Ma. The mineral assemblage and thermobarometry calculations indicate that the Oligocene metamorphism occurred under medium-pressure (MP) amphibolite-facies conditions (5.4–7.2 kbar, 691–765 °C). We propose that the Dongjiu gneisses represent the Precambrian metamorphic basement of the Lhasa terrane, ~~the oldest basement rocks so far recognized,~~ but have been intensively reworked by metamorphism in the SLT in response to the continued India-Asia convergence since the collision.

Keywords:

Zircon and Titanite *in situ* U–Pb dating; Mesoproterozoic; Precambrian metamorphic basement; Reworking; Lhasa terrane

1. Introduction

Like much of the central and southeastern Asian geology, the Tibetan Plateau formed via amalgamation of terranes during the Phanerozoic (Chang and Zheng, 1973; Allégre et al., 1984; Chang et al., 1986; Sengör and Natal'in, 1996; Yin and Nie, 1996). However, our knowledge on the histories of these terranes prior to their amalgamation remains limited. The early history of these terranes that make up the Tibetan Plateau is obscured by the paucity of basement exposure, by the strong reworking of basement rocks during the later thermal events, and by the predominance of younger supracrustal rocks~~ with strong reworking of later thermal events~~.

As the main tectonic component of the Tibetan Plateau, the Lhasa terrane has been considered to be composed dominantly of Paleozoic to Mesozoic strata, Mesozoic and Cenozoic igneous rocks and Precambrian basement (e.g.,~~,~~ Yin and Harrison, 2000; Pan et al., 2004, 2006). The nature and spatial distribution of the Precambrian basement beneath the entire terrane have~~has~~ been speculative. The limited works on the basement to date suggest that the Lhasa terrane crust is relatively young (< 2.0~~1.5~~ Ga). U–Pb dating of zircons in gneissic rocks shows the presence of the Neoproterozoic crystalline crust in the Amdo block (~ 850 ~~and 500~~ Ma, Guynn et al., 2006, 2012; Zhang et al., 2012a) and in the Xainza area in the central Lhasa subterrane (CLT) (~ 925–760 Ma, Hu et al., 2005; Zhang et al., 2012b; Hu et al., 2018a, b; Zeng et al., 2018). There is also Proterozoic~~Mesoproterozoic~~ crystalline basement in the Bomi area in the eastern CLT (ca. 1866 Ma,~~(~~~~~~~ 1343 ~~and~~ 1250 Ma and 824 Ma, Xu et al., 2013a; Chen et al., 2019) (Fig. 1a). These ages represent the only known Precambrian crystalline basement from the Lhasa terrane. Nd-Hf isotopic model ages have been used to suggest that the crust of the Lhasa terrane may be older, perhaps even Archean. Bulk-rock Nd isotope data on the Amdo Cambrian orthogneiss give Mesoproterozoic model ages (Harris et al., 1988a), while bulk-rock Nd and zircon Hf isotopic data on the Cretaceous granitoids of the Lhasa terrane yield Proterozoic and Archean model ages (Chiu et al., 2009; Zhu et al., 2009a). Zhu et al. (2011) suggest that the CLT was once a microcontinent with Proterozoic and Archean basement rocks, whereas the southern and northern parts of the Lhasa terrane are dominated by younger juvenile ~~granitoid~~ crust. However, zircon Hf isotopic mapping for the Mesozoic-Cenozoic magmatic rocks shows that the eastern segment of the northern Lhasa subterrane (NLT) is an ancient block; the southern Lhasa subterrane (SLT) is not entirely a juvenile block with inhomogeneity of crustal compositions (Hou et al., 2015). However, no Archean rocks have been identified so far. It is possible that the enriched radiogenic isotopic compositions could have resulted from the assimilation of melted sedimentary rocks that were themselves sourced from older continents (e.g.,~~.~~ Indian craton), rather than from pre-Neoproterozoic basement of the Lhasa terrane itself (Ding et al., 2003). Therefore, the true and complete constituent of the Precambrian basement beneath the Lhasa terrane remains to be revealed.

In this paper, we report the results of ~~our~~ petrological, geochronological and geochemical studies on reworked Precambrian metamorphic basement rocks from the Dongjiu area of the SLT (Fig. 1). The ~~Dongjiu~~ metamorphic rocks not only provide information on their protolith, but also record two episodes of subsequent metamorphism and Phanerozoic reworking of the Precambrian basement of the Lhasa terrane.

2. Geological setting and sample description

2.1. Geological setting

The Lhasa terrane on the southern segment~~margin~~ of the Tibetan Plateau is located between the Qiangtang terrane and Himalayan belt, bounded by the Bangong-Nujiang suture zone to the north and the Indus-Yarlung Zangbo suture zone to the south (Fig. 1a). From north to south, the Lhasa terrane has been divided into the northern, ~~(NLT),~~ central ~~(CLT)~~ and southern ~~(SLT)~~ subterranes, separated by the Shiquan River-Nam Tso mélange zone to the north and the Luobadui-Milashan fault to the south (Fig. 1a; Zhu et al., 2009a).

The NLT is characterized by the presence of juvenile crust and absence of a Precambrian basement (cf. Pan et al., 2004; Zhu et al., 2011). The sedimentary cover in the NLT is mainly Jurassic–Cretaceous with minor Triassic in age (e.g., Pan et al., 2004, 2006; Nimaciren et al., 2005). Voluminous Mesozoic volcanic rocks are exposed in this subterrane, and Mesozoic plutonic rocks are mainly confined to its western and eastern segments generally as huge batholiths (e.g., Zhu et al., 2011).

The CLT is covered with the widespread Permo-Carboniferous metasedimentary rocks, plus minor Ordovician, Silurian~~,~~ and Triassic strata (cf. Pan et al., 2004). The volcanic rocks in this subterrane are mostly early Cretaceous in age with minor being Permian. The Mesozoic plutonic rocks occur as batholiths of varying age (~ 215–88 Ma; cf. Zhu et al., 2011 and references therein). Cambrian volcanic rocks are scattered in the west and middle of the CLT (Fig. 1a, Zhu et al., 2012; Hu et al., 2013; Ding et al., 2015). The late Permian high-pressure eclogite and late Triassic–early Jurassic metamorphic rocks are exposed in the middle and eastern parts of the CLT (e.g., Yang et al., 2009; Zeng et al., 2009; Dong et al., 2011a; Lin et al., 2013a; Cheng et al., 2015; Weller et al., 2015; Chen et al., 2017). The Nyainqêntanglha Group in the middle part of the CLT has been interpreted as its Precambrian basement (Li, 1955; Allégre et al., 1984; Harris et al., 1988b; Pan et al., 2004). On the basis of zircon U–Pb dating, the protoliths of the Nyainqêntanglha Group near Xainza area were emplaced in the Neoproterozoic (Fig. 1a, Hu et al., 2005; Zhang et al., 2012b; Hu et al., 2018a, b; Zeng et al., 2018). Recent petrological studies with zircon U–Pb age data reveal that the rocks from the Xainza area are the relics of the Neoproterozoic (~ 900 Ma) ocean crust metamorphosed subsequently at ~ 690–650 Ma (Dong et al., 2011b; Zhang et al., 2012b). Moreover, Xu and co-workers (Xu et al., ~~. (~~2013a; Chen et al., 2019) reported the presence of Proterozoic~~Mesoproterozoic~~ basement with ~~a~~ crystallization ages~~age~~ of ca. 1866~~~ 1300~~ Ma, 1343–1250 Ma and 824 Ma from the Bomi complex in the southeastern ~~part of the~~ CLT. Chen et al. (2019) suggested that these Proterozoic gneisses revealed two metamorphic events at ca. 625–600 Ma and 80 Ma. These new data confirm the presence of a Precambrian metamorphic basement in the CLT.

The SLT is mainly composed of the Paleogene volcanic rocks, Cretaceous–Tertiary intrusions, Triassic–Cretaceous volcano-sedimentary rocks and minor medium- to high-grade metamorphic rocks (e.g., Pan et al., 2004; Zhu et al., 2008, 2013; Zhang et al., 2014a). The sedimentary cover in the SLT is largely restricted to its eastern segment (cf. Pan et al., 2004). The Nyingchi complex in the eastern SLT has been interpreted as the Precambrian basement (Pan et al., 2004; Yin et al., 2003; Xie et al., 2007). However, more recent studies indicated that most~~the~~ protoliths of the Nyingchi complex included both sedimentary and magmatic rocks of Cambrian (~ 496 Ma), Devonian (~ 360 Ma), Cretaceous (~ 90 Ma) and Eocene (~ 55 Ma), metamorphosed in the Mesozoic to Cenozoic (Dong et al., 2010, 2012, 2014; Guo et al., 2011, 2012; Palin et al., 2014; Xu et al., 2013b; Zhang et al., 2010, 2013, 2014a, b, 2015). Based on zircon U–Pb dating, Lin et al. (2013b) reported a metamorphic age of ~ 600 Ma from the Nyingchi complex in the eastern SLT, with a protolith age of ~ 1780 Ma. However, their samples are close to the northeast of the Eastern Himalayan Syntaxis, and are widely intruded by the Mesozoic–Cenozoic granitoids or occur as xenoliths within these granitoids (Lin et al., 2013b).~~gneisses in the eastern SLT.~~ Therefore, a Precambrian crystalline basement may indeed be present at least locally in the SLT.

The present~~Our~~ study area is located northwest of the Dongjiu area at the eastern edge of the SLT, where metamorphic rocks and Cenozoic intrusive rocks are exposed (Fig. 1b). The metamorphic rocks are offset by an east-west fault. The rocks north of the fault include schists and gneisses that experienced amphibolite-facies~~peak kyanite-grade~~ metamorphism at ~ 190 Ma (Chen et al., 2017). The studied samples are~~rocks in the south comprise~~ gneisses collected south of the fault.~~.~~ These metamorphic rocks are all intruded by the Cenozoic granites (~ 40–25 Ma; Booth et al., 2004).~~ The studied samples are gneisses collected south of the fault (Figs. 1b and 2).~~

2.2. Sample description

Sample details are given in Table 1, including protolith type, location, mineral assemblage, protolith and~~age,~~ metamorphic ages,~~age~~ and metamorphic *P–T* conditions.

The biotite-amphibole (Bt-amp) gneisses consist of plagioclase (~30 vol%), K-feldspar (~15 vol%), quartz (~35 vol%), amphibole (~10 vol%), biotite (~5 vol%), titanite (~3 vol%), allanite (~1 vol%), and accessory phases including epidote, ilmenite, apatite, rutile and zircon (Fig. 2a~~3a–~~d). The biotite~~Biotite~~ (Bt) gneisses are comprised of plagioclase (~20 vol%), K-feldspar (~35 vol%), quartz (~40 vol%), biotite (~4 vol%), and accessory minerals of allanite, epidote, apatite and zircon (Fig. 2e~~3e~~, f). The foliation is defined by aligned biotite flakes and quartz-feldspar bands. Thereinto, allanite occurs in two ways: those with~~replaced by~~ epidote ~~at~~ rims and zircon inclusions (Fig. 2c~~3c–~~e), ~~including zircon grains (Fig. 3c, d),~~ and those as inclusions within titanite (Fig. 7f~~8f~~, g, m, o, p). Most titanite grains rim~~are rimmed by~~ ilmenite, and some have inclusions of biotite, allanite, apatite, plagioclase, quartz or minor~~miner~~ rutile. The gneisses have a~~petrography shows the~~ mineral assemblage of plagioclase + K-feldspar + biotite + quartz + epidote ± amphibole ± titanite.

The studied gneisses underwent partial melting as revealed by the following evidence:~~presence of prior melt along grain boundaries is evident on thin-section~~

~~scales, such as~~ (1) feldspar grains with cuspate extensions along quartz-quartz contacts (Fig. 2b~~3b~~), (2) narrow trains of K-feldspar blebs along quartz-plagioclase contacts (Fig. 2a~~3a~~, f), (3) adjacent grains of quartz, feldspar and biotite ~~grains~~ are corroded (Fig. 2a~~3a~~, b, e, f). These microstructures are interpreted as crystallization products~~pseudomorphs~~ of the former ~~presence of~~ melt (e.g., Sawyer, 2001; Brown, 2002; Timmermann et al., 2002).

3. Analytical methods and results

Analytical method details are given in Supplementary Text 1, including Cathodoluminescence (CL) images, back scattered electron (BSE) images and analytical data on mineral major elements, bulk-rock major and trace elements, Sr–Nd isotopes, zircon U–Pb dating, trace elements and Hf isotopes, and titanite *in situ* U–Pb dating.

3.1. Mineral major element data

Major element compositions of plagioclase and amphibole in the ~~(~~Bt-amp gneiss (samples 169-1 and 39-1) are given in Supplementary Table 1 and 2, respectively.

Plagioclase grains in both samples are oligoclase, with An contents of 0.28–0.30. Amphibole grains have 10.98–11.68 wt% CaO and 1.19–1.42 wt% Na_2O classified as calcic amphibole (Leake et al., 1997).

3.2. Bulk-rock major and trace element and Sr–Nd isotope data

Bulk-rock major element, trace element and Sr–Nd isotopic compositions on the studied samples are given in Table 2.

The Bt-amp gneiss samples (169-1, 169-2 and 39-1) have 64.2–68.4 wt% SiO_2, 15.0–15.7 wt% Al_2O_3, 3.33–3.80 wt% CaO, 3.40–4.10 wt% Na_2O and 2.40–3.72 wt% K_2O. The Bt gneiss samples (168-1 and 169-4) are characterized by higher SiO_2 (70.3–71.9 wt%) and K_2O (4.33–5.34 wt%), but lower Al_2O_3 (13.9–14.7 wt%), CaO (1.85–2.06 wt%) and Na_2O (3.21–3.38 wt%). Using the Ab-An-Or classification for silicic rocks (Barker, 1979), the Bt-amp gneisses are granodiorite whereas the Bt gneisses are granite (Fig. 3a~~4a~~). These granitoid gneisses are metaluminous (Fig. 3b~~4b~~), with the aluminum saturation indices (A/CNK = molecular Al_2O_3 / (CaO + Na_2O + K_2O)) of 0.95–1.02.

These orthogneisses are enriched in light rare earth elements (REE) and relatively depleted in heavy REEs with highly fractionated REE patterns ($(La/Yb)_N$ = 15.3–143.5) and a weak negative Eu anomaly (Eu/Eu* = 0.62–0.87) (~~$((La/Yb)_N$ = 15.3–143.5;~~ Fig. 4a~~5a~~, Table 2). Furthermore, most samples display characteristic arc-like signature of negative Nb, Ta and Ti anomalies (except for sample 169-2 without Ti anomaly due to low REE contents, Fig. 4b~~5b~~).

For the analyzed four samples, their initial $^{87}Sr/^{86}Sr$ isotopic ratios and $\varepsilon_{Nd}(t)$ values calculated at t = 1520 Ma (see 3.3 below). The Bt-amp gneiss samples (169-1, 169-2 and 39-1) have ~~relatively high~~ initial $^{87}Sr/^{86}Sr$ ratios of 0.7008–0.7036 and $\varepsilon_{Nd}(t)$ values of -3.6 to +0.1, with model ages T_{DM2} = 2.35–2.05 Ga. The Bt gneiss sample (168-1) gives $\varepsilon_{Nd}(t)$ = -2.2 and T_{DM2} = 2.24 Ga, with an abnormally low $^{87}Sr/^{86}Sr_{initial}$ = 0.6866. This unusual~~ (Note that this initial Sr~~ isotopic ratio has no petrogenetic significance because of the mobility of Rb, which led to the excessive subtraction of $^{87}Rb/^{86}Sr$ ratio.~~Sr).~~

3.3. Zircon U–Pb age and Hf isotope

LA-ICP-MS zircon U–Pb dating and trace element analysis of five samples and zircon Hf isotope compositions of four samples are given in Supplementary Tables 3 and 4, respectively.

Zircon grains from the five gneisses are ~~mostly~~ colorless, subhedral–euhedral oblong or prismatic with varying size of ~ 100–200 µm. CL images show that zircon grains have a core–rim structure consisting of inherited cores with oscillatory zoning and dark rims with weak or no zoning (Figs. 5~~6~~ and 6). The~~7). All the~~ analyzed spots on zircon cores from two Bt-amp gneiss samples (169-1 and 169-2) and two Bt gneiss samples (168-1 and 169-4) yield weighted mean $^{207}Pb/^{206}Pb$ ages of 1519±36 Ma (n = ~~=~~5, MSWD = ~~=~~0.016), 1520±18 Ma (n = ~~=~~12, MSWD = ~~=~~0.85), 1516±15 Ma (n = ~~=~~20, MSWD = ~~=~~0.046) and 1506±6 Ma (n = ~~=~~16, MSWD = ~~=~~0.45), with upper intercept ages of 1544±47 Ma, 1551±23 Ma, 1544±26 Ma and 1498±6 Ma, respectively (Figs. 5a~~6a~~, c and 6a~~7a~~, c). All analyzed spots on core domains have relatively high Th contents (57.7–927 ppm), Th/U ratios (0.10–1.52) and REE contents (170–1576 ppm) with remarkable negative Eu anomalies (Eu/Eu* = ~~*=~~0.07–0.55) (~~;~~ Figs. 5b~~6b~~, d and 6b, d, Supplementary Tables 3~~7b, d~~). Analyzed spots on zircon rims from three Bt-amp gneiss samples (169-1, 169-2 and 39-1) and one Bt gneiss sample (168-1) yield weighted mean $^{206}Pb/^{238}U$ ages of 605±27 Ma (n = ~~=~~15, MSWD = ~~=~~0.96), 591±3 Ma (n = 14~~=15~~, MSWD = ~~=~~0.54) and 595±2 Ma (n = ~~=~~21, MSWD = ~~=~~0.40), with lower intercept ages of 585±11 Ma, 592±18 Ma, 588±6 Ma and 563±10 Ma, respectively (Figs. 5a~~6a~~, c, e and 6a~~7a~~). Only one zircon rim spot from sample 169-2 is obtained with $^{206}Pb/^{238}U$ age of 590±2 Ma (Figs. 5c~~6c~~). Compared with zircon cores, analyzed spots on rim domains have relatively low Th contents (22.0–82.2 ppm), Th/U ratios (0.03–0.10) and REE contents (50.3–473 ppm), with weak or no negative Eu anomalies (Eu/Eu* = ~~*=~~0.21–1.86) (~~;~~ Figs. 5b~~6b~~, d, f and 6a, Supplementary Tables 3~~7a~~).

Therefore, the zircon LA–ICP–MS U–Pb analyses yield two age groups: 1520–1506 Ma of weighted mean $^{207}Pb/^{206}Pb$ age for zircon cores and 605–590 Ma of weighted mean $^{206}Pb/^{238}U$ age for zircon rims.

Fifty-three Hf isotopic analyses on zircon cores from two Bt-amp gneiss samples (169-1 and 169-2) and two Bt gneiss samples (168-1 and 169-4) give initial $^{176}Hf/^{177}Hf$ isotopic ratios of 0.281697–0.281891 and $\varepsilon_{Hf}(t)$ values ranging from -4.5 to +2.6, with two-stage model ages T_{DM2} of 2.54–2.10 Ga (Supplementary Tables 4).~~.~~

3.4. Titanite *in situ* U–Pb age

Two titanite-rich gneiss samples (169-1 and 39-1) were selected for LA-ICP-MS titanite *in situ* U–Pb dating. BSE images and photomicrographs of representative titanite are shown in Fig. 7~~8~~ and the titanite U–Pb dating and trace element data are given in Supplementary Table 5.

Most titanite crystals are brown and subhedral–anhedral in shape with inclusions of ilmenite, biotite, allanite, apatite, plagioclase, quartz and minor~~miner~~ rutile (Fig. 7~~8~~). BSE images show that the titanite crystals mostly have patchy zoning. The analyzed spots of titanite yield lower intercept ages are 25.1±0.6 Ma for sample 169-1 (Fig. 8a~~9a~~) and 24.7±0.5 Ma for sample 39-1 (Fig. 8b~~9b~~). After correction using ^{207}Pb, the weighted mean $^{206}Pb/^{238}U$ ages are 26.2±0.4 Ma (n=40, MSWD=2.5) and 26.0±0.6 Ma (n=29, MSWD=3.1) (Fig. 8~~9~~).

4. Metamorphic *P–T* conditions

4.1. Hbl-Pl-Q thermobarometry

Amphibole–plagioclase thermometry (Holland and Blundy, 1994) and amphibole–plagioclase–quartz barometry (Bhadra and Bhattacharya, 2007) are used to calculate the ~~peak-~~metamorphic *P–T* condition of the Bt-amp gneisses. The amphibole–plagioclase–quartz~~Hbl-Pl-Q~~ thermobarometry yields metamorphic *P–T* conditions of 6.2–7.2 kbar and 691–736 °C for sample 169-1, and 5.4–6.5 kbar and 716–765 °C for sample 39-1.

4.2. Zr-in-titanite thermometry

Titanite~~For comparison, titanite~~ formation temperatures are~~were~~ estimated using the Zr-in-titanite thermometry (T (°C) = [7708 + 960P] / [10.52 − log(α_{TiO2}) −

log(α_{SiO2}) − log(ppm Zr, titanite)] − 273; Hayden et al., 2008). The activity of TiO_2 is assumed to be 0.5 (plausible lower limits in typical crustal rocks), with SiO_2 activity assumed as 1.0 (Hayden and Watson 2007; Ferry and Watson 2007). Based on amphibole–plagioclase–quartz~~Hbl-Pl-Q~~ barometer, the metamorphic pressure conditions of the Bt-amp gneisses are ~ 6 kbar. Zr concentrations range from 158 to 591 ppm in sample 169-1, and from 276 ppm to 620 ppm in sample 39-1. The calculations of Zr-in-titanite thermometry are 688–756 °C for sample 169-1 and 716–759 °C for sample 39-1 (Supplementary Table 5). The temperature data display a cluster at 700–750 °C (64/69, Fig. 9~~10~~), which is consistent with the ~~peak~~ temperature conditions obtained by the amphibole~~Amphibole~~–plagioclase thermometry.

5. Discussion

5.1. Age interpretation

Zircon LA-ICP-MS U–Pb dating shows two age groups of 1520–1506 Ma and 605–590 Ma. Most zircons of the studied Dongjiu gneisses show euhedral-prismatic forms and display rounded terminations, which in some cases generate an ovoid morphology. CL images show that all zircon grains have a core–rim structure, i.e., oscillatory-zoned core and rim with ~~no or~~ weak or no zoning (Figs. 5~~6~~ and 6~~7~~). The inherited zircon cores yield concordant ages of 1520–1506 Ma without detrital age distribution (analyses with concordance > 95%, Supplementary Tables 3). These zircon cores have relatively high Th contents (usually > 50 ppm) with high Th/U ratios (≥ 0.1, up to 1) (Fig. 10~~11~~) and REE patterns with remarkable negative Eu anomalies (Figs. 5b~~6b~~, d and 6b~~7b~~, d). These properties are consistent with the zircons ~~being~~ of magmatic origin (e.g., Hoskin and Schaltegger, 2003). Thus, the Mesoproterozoic age~~ages~~ of ~ 1500 Ma given by the zircon cores represents~~represent~~ the protolith crystallization age of the gneisses. By comparison, CL images show that zircon rims have ~~no or~~ weak or no zoning. Most zircon rims occur as lobes with smooth or rough edges, and may overprint pre-existing structures (Fig. 5b~~6b~~, f). All these characteristics suggest that ~~most~~ zircon rims have developed during metamorphic recrystallization near the solidus (Hoskin and Black, 2000; Rubatto, 2017). The zircon rims have lower Th contents (usually < 50 ppm) and Th/U ratios (< 0.1) (Fig. 10~~11~~) without remarkable negative Eu anomalies (Figs. 5b~~6b~~, d, f and 6b~~7b~~), which are ~~indeed~~ consistent with ~~being of~~ metamorphic zircon~~origin~~ (e.g., Rubatto et al., 2009; Rubatto, 2017). Based on the zircon internal structure, Th/U ratios and REE patterns, we suggest that the zircon rims provide the metamorphic ages of 605–590 Ma for the orthogneisses in the Dongjiu area ~~in the SLT~~.

Titanite crystals from two Bt-amp gneiss samples are ~~all~~ subhedral–anhedral in shape with metamorphic mineral inclusions of ilmenite, biotite, allanite, plagioclase, quartz or minor~~miner~~ rutile (Fig. 7~~8~~). BSE images show that titanite crystals have patchy zonation, characteristic of metamorphic titanite (Rubatto, 2017). Therefore, LA–ICP–MS titanite *in situ* U–Pb dating indicates that these gneisses experienced Oligocene~~recent~~ metamorphism at ~ 26 Ma.

In summary~~conclusion~~, the protoliths~~protolith~~ of the gneisses from the Dongjiu area~~ of the SLT~~ crystallized in the Mesoproterozoic (1520–1506 Ma), and followed by subsequent metamorphism in the Neoproterozoic (605–590 Ma) and more recently in the Oligocene (~ 26 Ma).

5.2. Mesoproterozoic magmatism

The Lhasa terrane, as the southernmost part of the Asian continent, experienced intense deformation, magmatism and metamorphism related to the northward Neo-Tethyan seafloor subduction in the Mesozoic and the India-Asia continental collision in the Cenozoic (e.g., Zhu et al., 2011; Zhang et al., 2014a). Due to these strong reworking processes, the Precambrian thermotectonic records are rarely reported (e.g., Dong et al., 2010, 2011b; Guynn et al., 2012; Zhang et al., 2012b; Xu et al., 2013a; Hu et al., 2018b; Chen et al., 2019).

Based on the zircon U–Pb geochronology, the inherited magmatic zircon cores of the Dongjiu gneisses yield crystallization ages of 1520–1506 Ma (lack detrital components; see above), indicate that the protoliths of Dongjiu gneisses are Mesoproterozoic magmatic rocks. The bulk-rock chemical compositions of the Dongjiu gneisses suggest that their protoliths are metaluminous granodiorite and granite (Fig. 34), characteristic of arc-like signature with negative Nb, Ta and Ti anomalies (Fig. 4b~~5b~~). The Mesoproterozoic granitic rocks have bulk-rock $\varepsilon_{Nd}(t)$ values of -3.6 to +0.1 and zircon $\varepsilon_{Hf}(t)$ values of -4.5 to +2.6, with similar T_{DM2} ages of 2.35–2.05 Ga and 2.54–2.10 Ga~~,~~ respectively, suggesting that the magmatic rocks are derived from partial melting of Paleoproterozoic crustal material.

The coeval ~ 1500 Ma magmatic rocks are widespread in several continental fragments~~ in different tectonic settings~~, including West Africa, South America, North America, Australia, Baltica (Northern Europe), Siberia and India. The rock types are mainly mafic dikes and sills (e.g., Ernst et al., 2013, 2016; Silveira et al., 2013), and massif-type anorthosites (e.g., Emslie, 1978; Weis, 1986; Sadowski and Bettencourt, 1996; Mukherjee and Das, 2002). The Mesoproterozoic Era, dominated by the break-up of the Columbia supercontinent and the formation of the Rodinia supercontinent, was an important crust-forming period in many continents in Earth's history. The global Mesoproterozoic magmatism has commonly been attributed to the rifting and fragmentation of the Columbia supercontinent (e.g., Rogers and Santosh, 2002; Zhao et al., 2003). However, ~ 1.6–1.5 Ga metamorphic and magmatic rocks of the Central Indian Tectonic Zone are the products of south-north Indian subcontinental collision (e.g., Acharyya, 2003; Kröner et al., 2012). For the studied Mesoproterozoic granitic rocks in the SLT, it is too~~ early and~~ difficult to discuss the tectonic setting in a global context owing to their limited distribution and subsequent reworking.

The Mesoproterozoic inherited zircons in the Gangdese batholith (e.g., Zhu et al., 2011; Ji et al., 2017), and detrital zircons from the sedimentary rocks of the Carboniferous–Triassic strata (Leier et al., 2007; Pullen et al., 2008; Dong et al., 2010; Zhu et al., 2013; Li et al., 2014; Guo et al., 2017) indicate that the Mesoproterozoic magmatic rocks are probably more widely distributed than exposed in the Lhasa terrane. Moreover, the metasedimentary rocks from the Nyingchi complex in the SLT contain abundant ~1500 Ma detrital zircons (Guo et al., 2017).

The 1550–1450 Ma detrital zircons from the CLT Permian–Triassic strata define a broad band of $\varepsilon_{Hf}(t)$ values (-16.7 to +9.6; Fig. 11~~12~~). By comparison, the coeval detrital zircons from the SLT metasedimentary rocks have lower $\varepsilon_{Hf}(t)$ values (-11.3 to +3.2; Fig. 11~~12~~). The studied Mesoproterozoic granitic rocks, with the coeval gneisses of the southern Nyingchi complex (our unpublished data) have the similar zircon $\varepsilon_{Hf}(t)$ values as the above, suggesting that they might be local sources for the Mesoproterozoic detrital zircons of the Paleozoic strata (Fig. 11~~12~~).

5.3. Neoproterozoic and Oligocene metamorphism

Based on zircon and titanite U–Pb geochronology, the Dongjiu orthogneisses experienced two metamorphic events at 605–590 Ma recorded by zircon and 26 Ma by titanite, respectively.

5.3.1. Neoproterozoic metamorphism

Due to the Oligocene metamorphism, the Neoproterozoic metamorphic minerals are usually overprinted. The petrography shows that ilmenite is all surrounded by titanite; rare rutile only occurs as inclusions within titanite; and allanite is rimed by epidote including zircon grains (Figs. 2c~~3c~~, d and 7~~8~~). Along with titanite formed in the later metamorphism, we speculate that the mineral assemblage of the Neoproterozoic metamorphism is represented as ilmenite and allanite. Lacking index metamorphic minerals, it is difficult to calculate the detailed *P*–*T* conditions of the Neoproterozoic metamorphism for the studied gneisses. However, the characteristics of zircon internal structure and chemistry show that zircon rims of the Dongjiu gneisses likely form under conditions near solidus. Rubatto et al. (2009) show that the metamorphic zircon rims of metatonalite with the similar mineral assemblage to this study formed under amphibolite-facies condition (T = 620–700 ºC). For diorite bulk composition, recent phase equilibrium modeling indicated that the H_2O-saturated (wet) solidus occurs between ~ 650–700 °C and garnet becomes stable above ~ 8.5 kbar (e.g., Palin et al., 2016). On the formation condition of zircon rim, bulk composition and lack of garnet, we reason~~speculate~~ that the Dongjiu granitic gneisses underwent MP~~medium-pressure~~ amphibolite-facies metamorphism at 605–590 Ma.

According to the Gondwana-derived affinity, the ~ 600 Ma metamorphic event of the Lhasa terrane is likely related to the assembly of Gondwana supercontinent (e.g., Meert, 2003; Veevers, 2004; Collins and Pisarevsky, 2005). Early palaeogeographic models based on limited data interpreted the presence of a single super-continent throughout the Proterozoic (Piper, 1976). McWilliams (1981) suggested that two Neoproterozoic continental masses, East Gondwana (India, East Australia, Antarctica, Madagascar and Sri Lanka) and West Gondwana (Africa and South America) collided along the Mozambique Belt to form Gondwana. Form the Rodinia fragments to the final amalgamation Gondwana, there have been many accretionary terranes and collisional events (Collins and Pisarevsky, 2005). Although more work is needed on details of such amalgamation. Meert and co-workers (Meert, et al., 1995; Meert and Van der Voo, 1997; Meert, 2001, 2003) suggested a multiphase assembly of two main periods of orogenesis, including an earlier East

African Orogeny (EAO) (~ 750–620 Ma) and a later Kuunga Orogeny (~ 570–530 Ma). The later orogeny marks the collision of Australia and Antarctica with the rest of Gondwana and was subsequently correlated with a broad belt of orogenesis from the Damara Orogen in the west to the Pinjarra Orogen in the east (Meert, 2003). They proposed a Neoproterozoic continent consisting of Sri Lanka, Madagascar and India colliding with a combined Congo/Kalahari (African) continent at ~ 750–620 Ma, followed by Australia/East Antarctica colliding with the bulk of Gondwana at ~ 570–530 Ma (Meert, 2003; Meert and Torsvik, 2003). However, Boger and Miller (2004) proposed that the EAO evolved as an accretionary orogeny and was partially superimposed by a ~ 590–560 Ma orogen created by the collision of combined India, Madagascar and part of Antarctica land masses with eastern Africa along the Mozambique suture. In their model, Australia–Antarctica collided with India along the Kuunga suture at ~ 535–520 Ma. Until now, the Precambrian metamorphic events of the Lhasa terrane are only reported in the Nyainqêntanglha Group in the central CLT (~ 690–650 Ma, Dong et al., 2011b; Zhang et al., 2012b), the Bomi complex in the eastern CLT (~ 625–600 Ma, Chen et al., 2019), and the Nyingchi complex in the eastern SLT (~ 600 Ma, Lin et al., 2013b and this study). The Nyainqêntanglha Group experienced an early granulite-facies peak-metamorphism at ~ 690–650 Ma, and late amphibolite-facies retrogression at ~ 480 Ma (Dong et al., 2011b; Zhang et al., 2012b). Zhang et al. (2012b, 2014a) suggested that the Neoproterozoic metamorphism occurred during the assembly of East and West Gondwana within the EAO. For all other Precambrian metamorphic events, only the Nyingchi complex is speculated to experience MP amphibolite-facies metamorphism without knowing exact *P–T* conditions due to the Cenozoic metamorphic reworking. Therefore, this study suggests that the ~ 600 Ma metamorphism events recorded in the Nyingchi complex in the eastern SLT and the Bomi complex in the eastern CLT are likely response to the assembly of Gondwana supercontinent.

5.3.2. Oligocene metamorphism and melting

In this study, titanite formed at ca.~~~~~ 26 Ma is observed either mostly riming ilmenite or as separate grains. Titanite can be in contact with a variety of minerals, e.g.,~~.~~ amphibole, biotite, plagioclase and epidote, and contains inclusions of biotite, allanite, plagioclase and quartz (Fig. 7~~8~~). The formation of titanite rims on the ilmenite could be explained in terms of reactions such as: ilmenite + allanite + K-feldspar + quartz = titanite + anorthite + annite + H_2O (Harlov et al., 2006; Angiboust and Harlov, 2017). Titanite rimming ilmenite is commonly present in the amphibolite-facies rocks (e.g., Nijland and Maijer, 1993; Nijland and Visser, 1995; Hansen et al., 2002; Harlov and Hansen, 2005). The mineral assemblage (plagioclase + K-feldspar + biotite + quartz + epidote ± amphibole ± titanite) also indicates that the later Oligocene metamorphism occurred at amphibolite-facies condition. Hbl-Pl-Q thermobarometry shows that the Dongjiu gneisses experienced peak *P–T* conditions of 5.4–7.2 kbar and 691–765 °C. Zr-in-titanite thermometry yields the similar *T* conditions of 688–759 °C at ~ 6 kbar. Moreover, the microstructure proves that these studied gneisses record the presence of melt.~~ along grain boundaries.~~ Therefore, we suggest that the prior ~~presence of~~ melt represents~~represent~~ the product of the Oligocene metamorphism, and the Dongjiu ~~granitic~~ gneisses underwent MP~~medium-pressure~~ amphibolite-facies metamorphism and melting at ca.~~~~~ 26 Ma. In the southern part of the studied area, the coeval metamorphic rocks of the Nyingchi complex have also been reported to take place under amphibolite-facies conditions (e.g., Zhang et al., 2010; Dong et al., 2012; Palin et al., 2014; Kang et al., 2019).

5.4. The nature of the Precambrian basement of the Lhasa terrane

The spatial distribution and nature of the Precambrian basement beneath the entire Lhasa terrane have~~has~~ been speculative. Duo to medium- to high-grade metamorphism, the Nyainqêntanglha Group in the CLT and the Nyingchi complex in the SLT have been regarded as the Precambrian metamorphic basement (Xu et al. 1985; Dewey et al. 1988; Harris 1988b; Hu et al. 2005). However, adequate age constraints are lacking. Based on zircon Hf isotope data, Zhu et al (2011) suggested that the CLT has ancient basement rocks of Proterozoic and Archean ages with NLT and SLT being younger and juvenile crust (Phanerozoic) accreted towards the CLT.

The Amdo basement, consisting of orthogneisses and mafic granulites, is reported to represent the Precambrian basement of the Lhasa terrane (Xu et al., 1985; Coward et al., 1988; Kidd et al., 1988; Pan et al., 2004). The gneisses have crystallization ages of Neoproterozoic (~820 Ma; Zhang et al., 2012a) and Cambro-Ordovician (540–460 Ma; Xu et al., 1985; Xie et al., 2010; Guynn et al., 2012; Zhang et al., 2012a). The mafic granulites have undergone~~underwent~~ peak granulite-facies metamorphism at ~ 190 Ma and retrogressed under amphibolite-facies conditions at ~ 180 Ma (e.g., Xu et al., 1985; Guynn et al., 2006; Zhang et al., 2012a; Zhang XR et al., 2014). Therefore, the Amdo gneiss represents a Neoproterozoic crystallization basement, which undergoes~~underwent~~ metamorphism in the early Jurassic.

The existence of a Precambrian basement in the CLT has been previously inferred using older inherited zircon ages of the gneiss (Allégre et al., 1984) and the bulk-rock Nd isotope composition from sedimentary rocks (Zhang KJ et al., 2007). Recently reported old rocks are the ca.~~~~~ 925–748 Ma granitoids and gabbros of the Nyainqêntanglha Group in the Xianza area west of Nam Tso Lake (Hu et al., 2005; Zhang et al., 2012b; Hu et al., 2018 a, b; Zeng et al., 2018). These rocks have experienced ~~amphibolite- to~~ granulite-facies peak-metamorphism at ca. 690~~~ 680~~–650 Ma ~~and 480 Ma~~ (Dong et al., 2011b; Zhang et al., 2012b). Some studies suggest that the Neoproterozoic magmatic rocks are crust of the Mozambique Ocean (Zhang et al., 2012b; Zeng et al., 2018), but others propose that these rocks formed in a back-arc setting (Hu et al., 2018 a, b). In addition, the Bomi complex consists of the Proterozoic magmatic rocks formed at ca. 1866 Ma, 1343–1250 Ma and 824 Ma, and undergoes metamorphism at ca. 625–600 Ma and 80 Ma (Xu et al., 2013a; Chen et al., 2019). Thereinto, the Paleoproterozoic and Neoproterozoic granitoid gneisses show geochemical affinity of volcanic arc granites (Chen et al., 2019); the Mesoproterozoic granite gneisses have an aluminous A-type granite affinity (Xu et al., 2013a). However, there is no constraint on the metamorphic condition. Therefore, the CLT indeed has~~In addition, Xu et al. (2013a) reported ~ 1343 and 1250 Ma A-type granites~~

~~in the eastern CLT. These Mesoproterozoic granitoids have zircon T_{DM2} ages of 2.1–1.4 Ga, suggesting that CLT may have~~ Proterozoic basement.

In the SLT, the Nyingchi complex has been interpreted to represent slivers of a Precambrian basement of the Lhasa terrane (e.g., Pan et al., 2004; Xie et al., 2007; Yin et al., 2003). However, more recent studies suggested that most~~some~~ high-grade metamorphic rocks in the eastern SLT underwent Mesozoic to Cenozoic metamorphism and their protoliths included both sedimentary and magmatic rocks with various protolith ages (Dong et al., 2010, 2012, 2014; Guo et al., 2011, 2012, 2017; Palin et al., 2014; Xu et al., 2013b; Zhang et al., 2010, 2013, 2014a, 2014b, 2015). Here, the Dongjiu gneisses, as a part of the Nyingchi complex, have a protolith crystalline age of 1520–1506 Ma, and experienced amphibolite-facies metamorphism at 605–590 Ma, representing a Precambrian metamorphic basement of the SLT. Moreover, the studied Mesoproterozoic granitic rocks have T_{DM2} of 2.54~~5~~–2.10 Ga, along with Meso- to Paleoproterozoic zircon Hf model ages of Cambrian and Devonian–Carboniferous granitoids (Ji et al., 2012; Dong et al., 2014, 2015),~~1 Ga,~~ implying the presence of an older early Paleoproterozoic curst yet unidentified in the SLT.

Excluding~~Until now,~~ the ca. 1780 Ma xenoliths reported by Lin et al. (2013b), the ~ 1500 Ma granitic gneisses from the Dongjiu area ~~we report~~ here are the oldest rocks reported of the SLT.~~Lhasa terrane.~~ The zircon Hf and bulk-rock Nd isotopes give similar T_{DM2} ages up to 2.5 Ga, suggesting that the Mesoproterozoic granitic rocks are derived from melting of the Paleoproterozoic crustal material. ~~By contrast,~~

~~the ~1300 Ma granitoids from the CLT have younger zircon Hf T_{DM2} age of 2.0–1.4 Ga.~~ Moreover, the ~ 1500 Ma gneisses from the southern Nyingchi complex give Paleoproterozoic zircon Hf model ages (Fig. 11, our ~~(~~unpublished data). By comparison, the Proterozoic granitoids from the Bomi complex in the CLT have similar zircon Hf T_{DM2} ages ranging from 2.5 to 1.~~) give zircon Hf T_{DM2} age of 2.~~3 Ga (Xu et al., 2013a; Chen et al., 2019). Furthermore, the magmatic rocks (before 360 Ma) from both the SLT and CLT have the same ranges of zircon $\varepsilon_{Hf}(t)$ values and model ages (Fig. 11).~~–1.7 Ga.~~ Therefore, we suggest that~~either the SLT is heterogeneous with older Precambrian basement than the CLT or~~ the SLT and CLT share a common Precambrian basement.~~, but older rocks have not yet been identified in the CLT. We prefer the latter to be more likely because before 360 Ma, the magmatic rocks from both the SLT and CLT share the same $\varepsilon_{Hf}(t)$ range and the same range of model ages (Fig. 12).~~

5.5. Reworking of the Precambrian basement of the Lhasa terrane

Although both SLT and CLT share a common Precambrian basement, the strong thermal events (including metamorphism and mainly mantle-derived magmatism) as a consequence of the northward subduction of the Neo-Tethyan seafloor beneath the Lhasa terrane and the subsequent India-Asia continental collision have intensively reworked the Precambrian basement.

Since the early Mesozoic, important mantle contributions have caused the drastically elevated zircon $\varepsilon_{Hf}(t)$ of the magmatic rocks from the SLT (Fig 11~~12~~).

However, their zircon $\varepsilon_{Hf}(t)$ values vary significantly (up to 20 units from ~ -5 to +15; Fig. 11~~12~~), indicating the presence of old basement. The input of mantle material not only contributed to juvenile continental crust growth (e.g., Mo et al., 2007; Zhu et al., 2011), but also reworked the Precambrian basement of the SLT. In contrast, the granitoids from the CLT exhibit negative zircon $\varepsilon_{Hf}(t)$ and old T_{DM2} ages, suggesting that they are~~were~~ mainly derived from partial melting of ancient continental crust. Therefore, the basement of the CLT underwent weaker reworking, preserving more rocks with Nd-Hf isotopes characteristic of ancient continental crust than the SLT.

This study shows that the Precambrian metamorphic basement of the Lhasa terrane has also undergone more recent metamorphism at ~ 26 Ma. Due to similar metamorphic conditions, it is difficult to distinguish mineral assemblages as the result of recent metamorphism from those of the Neoproterozoic metamorphism, except for the preserved inclusions of ilmenite and allanite. The main mineral assemblage of plagioclase + K-feldspar + biotite + quartz + epidote ± amphibole ± titanite is the product of the Oligocene metamorphism. The coeval metamorphic rocks have been widely reported in the south part of the Nyingchi complex (e.g., Zhang et al., 2010, 2014a; Guo et al., 2011; Dong et al., 2012; Palin et al., 2014; Kang et al., 2019). Zhang et al. (2015) suggested that the crustal shortening and thickening resulting from the continental collision and continued convergence is the very tectonic~~physical~~ mechanism for the Oligocene reworking of the Lhasa terrane crust.

6. Conclusion

(1) The protoliths of the Dongjiu orthogneisses~~gneisses~~ in the SLT are granodiorite and granite emplaced at 1520–1506 Ma, which provide source materials for the Paleozoic metasedimentary rocks in the Lhasa terrane. The~~On the basis of crustal model ages using bulk-rock Nd and zircon Hf isotopes, we conclude that the~~ Mesoproterozoic granitoids~~ must~~ have derived from partial melting of earlier Paleoproterozoic crustal material.

(2) The Mesoproterozoic orthogneisses~~granitic gneisses~~ from the Dongjiu area have experienced the Neoproterozoic (605–590 Ma~~ on zircon U-Pb dating~~) metamorphism, and therefore represent the Precambrian metamorphic basement of the SLT.

(3) The Dongjiu gneisses also underwent the Oligocene (26 Ma~~ on titanite *in situ* U–Pb dating~~) metamorphism under MP~~medium-pressure~~ amphibolite-facies conditions as the result of crustal shortening and thickening in response to the continued India-Asia continental convergence.

(4) The CLT and SLT share a common Precambrian metamorphic basement, but the SLT basement has been strongly reworked by mantle-derived magmatism and metamorphism since the Mesozoic.

Acknowledgments

We want to thank two anonymous journal referees and Editor Guochun Zhao for their constructive comments, which have helped improve the quality of this paper. This study was supported by the National Natural Science Foundation of China (grants 41872070 and 91855210) and the ~~Geological Survey Project of the~~ China Geological Survey (grants DD20160122~~DD20160022~~ and DD20190057~~DD20160201~~). Xin Dong acknowledges the China Scholarship Council for funding a 12-month research at Durham University, UK (CSC NO. 201809110024). We thank Dr. Zhenyu He, Hua Xiang and Fenghua Liang for their support of this work; Dr.~~Ph.D. students~~ Zhengbin Gou and Huixia Ding for taking part in field work, and Ph.D. students Yanhong Chen and Fangyu Shen for helpful discussion.

References

Acharyya, S.K., 2003. The Nature of Mesoproterozoic Central Indian Tectonic Zone with Exhumed and Reworked Older Granulites. Gondwana Res. 6 (2), 197–214.

Allégre, C.J., et al., 1984. Structure and evolution of the Himalaya–Tibet orogenic belt. Nature 307, 17–22.

Angiboust, S., Harlov, D., 2017. Ilmenite breakdown and rutile-titanite stability in metagranitoids: Natural observations and experimental results. Am. Mineral. 102 (8), 1696–1708.

Barker, F., 1979. Trondhjemite: definition environment and hypothesis of origin. In: Barker F (Ed) Trondhjemites dacites and related rocks. Elsevier, Amsterdam, pp.

1–12.

Bhadra, S., Bhattacharya, A., 2007. The barometer tremolite + tschermakite + 2 albite = 2 pargasite + 8 quartz: constraints fromexperimental data at unit silica activity, with application to garnet-free natural assemblages. Am. Mineral. 92 (4), 491–502.

Boger, S.D., Miller, J.M., 2004. Terminal suturing of Gondwana and the onset of the Ross–Delamerian Orogeny: The cause and effect of an Early Cambrian reconfiguration of plate motions. Earth Planet. Sci. Lett. 219, 35–48.

Booth, A.L., Zeitler, P.K., Kidd, W.S.F., Wooden, J., Liu, Y.P., Idleman, B., Hren, M., Chamberlain, C.P., 2004. U–Pb zircon constraints on the tectonic evolution of southeastern Tibet, Namche Barwa area. Am. J. Sci. 304 (10), 889–929.

Brown, M., 2002. Retrograde processes in migmatites and granulites revisited. J. Metamorph. Geol. 20 (1), 25–40.

Chang, C.F., et al., 1986. Preliminary conclusions of the Royal Society and Academia-Sinica 1985 Geotraverse of Tibet. Nature 323, 501–507.

Chang, C.F., Zheng, S.L., 1973. Tectonic features of the Mount Jolmo Lungma region in southern Tibet, China. Chin. J. Geol. 1 (1), 1–12.

Chen, L.R, Xu, W.C., Zhang, H.F., Zhao, P.L., Guo, J.L., Luo, B.J., Guo, L., Pan, F.B., 2019. Origin and early evolution of the Lhasa Terrane, South Tibet: Constraints from the Bomi Gneiss Complex. Precambrian Res. 331, 105360.

Chen, Z.J., Tian, Z.L., Zhang, Z.M., Dong, X., 2017. Early Jurassic metamorphism of the eastern segment of the Lhasa terrane in south Tibet and its tectonic significance. Int. Geol. Rev. 59 (14), 1–17.

Cheng, H., Liu, Y., Vervoort, J.D., Lu, H., 2015. Combined U–Pb, Lu–Hf, Sm–Nd and Ar–Ar multichronometric dating on the Bailang eclogite constrains the closure timing of the Paleo-Tethys Ocean in the Lhasa terrane, Tibet. Gondwana Res. 28 (4), 1482–1499.

Chiu, H.Y., Chung, S.L., Wu, F.Y., Liu, D.Y., Liang, Y.H., Lin, Y.J., Iizuka, Y., Xie, L.W., Wang, Y.B., Chu, M.F., 2009. Zircon U–Pb and Hf isotope constraints from eastern Transhimalayan batholiths on the precollisional magmatic and tectonic evolution in southern Tibet. Tectonophysics 477 (1–2), 3–19.

Chu, M.F., Chung, S.L., Song, B., Liu, D.Y., O'Reilly, S.Y., Pearson, N.J., 2006. Zircon U–Pb and Hf isotope constraints on the Mesozoic tectonics and crustal evolution of southern Tibet. Geology 34 (9), 745–748.

Collins, A.S., Pisarevsky, S.A., 2005. Amalgamating eastern Gondwana: The evolution of the circum-Indian orogens. Earth Sci. Rev. 71, 229–270.

Coward, M.P., Kidd, W.F., Yun, P., Shackleton, R.M., Zhang, H., 1988. The structure of the 1985 Tibet Geotraverse, Lhasa to Golmud. Phil. Trans. Roy. Soc. Lond. A 327, 307–336.

Dewey, J.F., Shackelton, R.M., Chang, C., Sun, Y., 1988. The tectonic evolution of the Tibetan Plateau. Phil. Trans. Roy. Soc. Lond. A 327, 379–413.

Ding, H.X., Zhang, Z.M., Dong, X., Yan, R., Lin, Y.H., Jiang, H.Y., 2015. Cambrian ultrapotassic rhyolites from the Lhasa terrane, south Tibet: Evidence for Andean-type magmatism along the northern active margin of Gondwana. Gondwana Res.

27 (4), 1616–1629.

Ding, L., Kapp, P., Zhong, D., Deng, W., 2003. Cenozoic volcanism in Tibet: Evidence for a transition from oceanic to continental subduction. J. Petrol. 44, 1833–1865.

Dong, X., Zhang, Z.M., Santosh, M., 2010. Zircon U–Pb chronology of the Nyingtri Group, Southern Lhasa Terrane, Tibetan Plateau: Implications for Grenvillian and Pan-African provenance and Mesozoic-Cenozoic metamorphism. J. Geol. 118 (6), 677–690.

Dong, X., Zhang, Z.M., Liu, F., Wang, W., Yu, F., Shen, K., 2011a. Zircon U–Pb geochronology of the Nyainqêntanglha Group fromthe Lhasa terrane: New constraints on the Triassic orogeny of the south Tibet. J. Asian Earth Sci. 42 (4), 732–739.

Dong, X., Zhang, Z.M., Santosh, M., Wang, W., Yu, F., Liu, F., 2011b. Late Neoproterozoic thermal events in the northern Lhasa terrane, south Tibet: Zircon chronology and tectonic implications. J. Geodyn. 52 (5), 389–405.

Dong, X., Zhang, Z.M., Liu, F., Wang, W., Yu, F., Lin, Y.H., Jiang, H.Y., He, Z.Y., 2012. Genesis of the metamorphic rocks from southeastern Lhasa terrane and the Mesozoic-Cenozoic orogenesis. Acta Petrol. Sin. 28 (6), 1765–1784 (in Chinese with English abstract).

Dong, X., Zhang, Z.M., 2013. Genesis and tectonic significance of the Early Jurassic magmatic rocks from the southern Lhasa terrane. Acta Petrol. Sin. 29 (6), 1933–1948 (in Chinese with English abstract).

Dong, X., Zhang, Z.M., Liu, F., He, Z.Y., Lin, Y.H., 2014. Late Paleozoic intrusive rocks from the southeastern Lhasa terrane, Tibetan Plateau, and their Late Mesozoic metamorphism and tectonic implications. Lithos 198–199, 249–262.

Dong, X., Zhang, Z.M., 2015. Cambrian granitoids from the southeastern Tibetan Plateau: Research on petrology and zircon Hf isotope. Acta Petrol. Sin. 31 (5), 1183–1199 (in Chinese with English abstract).

Emslie, R.F., 1978. Anorthosite massifs, rapakivi granites, and late Proterozoic rifting of North America. Precambrian Res. 7 (1), 61–98.

Ernst, R.E., Pereira, E., Hamilton, M.A., Pisarevsky, S.A., Rodriques, J., Tassinari, C.C.G., Teixeira, W., Van-Dunem, V., 2013. Mesoproterozoic intraplate magmatic ‘barcode’ record of the Angola portion of the Congo Craton: Newly dated magmatic events at 1505 and 1110 Ma and implications for Nuna (Columbia) supercontinent reconstructions. Precambrian Res. 230, 103–118.

Ernst, R.E., Okrugin, A.V., Veselovskiy, R.V., Kamo, S.L., Hamilton, M.A., Pavlov, V., Söderlund, U., Chamberlain, K.R., Rogers, C., 2016. The 1501 Ma kuonamka large igneous province of northern siberia: U–Pb geochronology, geochemistry, and links with coeval magmatism on other crustal blocks. Russ. Geol. Geophys. 57 (5), 653–671.

Ferry, J.M., Watson, E.B., 2007. New thermodynamic models and revised calibrations for the Ti-in-zircon and Zr-in-rutile thermometers. Contrib. Mineral. Petrol. 154 (4), 429–437.

Guo, L., Zhang, H.F., Harris, N., Pan, F.B., Xu, W.C., 2011. Origin and evolution of multistage felsic melts in eastern Gangdese belt: Constraints from U–Pb zircon dating and Hf isotopic composition. Lithos 127 (1–2), 54–67.

Guo, L., Zhang, H.F., Harris, N., Parrish, R., Xu, W.C., Shi, Z.L., 2012. Paleogene crustal anatexis and metamorphism in Lhasa terrane, eastern Himalayan syntaxis: Evidence from U–Pb zircon ages and Hf isotopic compositions of the Nyingchi Complex. Gondwana Res. 21 (1), 100–111.

Guo, L., Zhang, H.F., Harris, N., Xu, W.C., Pan, F.B., 2017. Detrital zircon U–Pb geochronology, trace-element and Hf isotope geochemistry of the metasedimentary rocks in the eastern Himalayan syntaxis: Tectonic and paleogeographic implications. Gondwana Res. 41, 207–221.

Guo, L.S., Liu, Y.L., Liu, S.W., Cawood, P.A., Wang, Z.H., Liu, H.F., 2013. Petrogenesis of Early to Middle Jurassic granitoid rocks from the Gangdese belt, Southern Tibet: Implications for early history of the Neo-Tethys. Lithos 179, 320–333.

Guynn, J.H., Kapp, P., Pullen, A., Heizler, M., Gehrels, G., Ding, L., 2006. Tibetan basement rocks near Amdo reveal “missing” mesozoic tectonism along the Bangong suture, central Tibet. Geology 34 (6), 505–508.

Guynn, J., Kapp, P., George, E., Ding, L., 2012. U–Pb geochronology of terrane rocks in central Tibet and paleogeographic implications. J. Asian Earth Sci. 43 (1), 23–50.

Hansen, E.C., Ahmed, K., Harlov, D.E., 2002. Rb depletion in biotites and whole rocks across an amphibolite to granulite-facies transition zone, Tamil Nadu, South India. Lithos 64 (1), 29–47.

Harlov, D.E., Hansen, E.C., 2005. Oxide and sulphide isograds along a late Archean, deep-crustal profile in Tamil Nadu, South India. J. Metamorph. Geol. 23 (4), 241–259.

Harlov, D.E., Tropper, P., Seifert, W., Nijland, T., Förster, H.J., 2006. Formation of Al-rich titanite ($CaTiSiO_4O$–$CaAlSiO_4OH$) reaction rims on ilmenite in metamorphic rocks as a function of fH_2O and fO_2. Lithos 88, 72–84.

Harris, N.B.W., Xu, R.H., Lewis, C.L., Hawkesworth, C.L., Zhang, Y.Q., 1988a. Isotope geochemistry of the 1985 Tibet Geotraverse, Lhasa to Golmud. Phil. Trans. Roy. Soc. Lond. A 327, 263–285.

Harris, N.B.W., Holland, T.J.B., Tindle, A.G., 1988b. Metamorphic rocks of the 1985 Tibet Geotraverse, Lhasa to Golmud. Phil. Trans. Roy. Soc. Lond. A 327, 203–213.

Hayden, L.A., Watson, E.B., 2007. Rutile saturation in hydrous siliceous melts and its bearing on Ti-thermometry of quartz and zircon. Earth Planet. Sci. Lett. 258 (3–4), 561–568.

Hayden, L.A., Watson, E.B., Wark, D.A., 2008. A thermobarometer for sphene (titanite). Contrib. Mineral. Petrol. 155 (4), 529–540.

Holland, T.J.B., Blundy, J.D., 1994. Non-ideal interactions in calcic amphiboles and their bearing on amphibole–plagioclase thermometry. Contrib. Mineral. Petrol. 116 (4), 433–447.

Hoskin, P.W.O., Black, L.P., 2000. Metamorphic zircon formation by solid-state recrystallization of protolith igneous zircon. J. Metamorph. Geol. 18 (4), 423–439.

Hoskin, P.W.O., Schaltegger, U., 2003. The composition of zircon and igneous and metamorphic petrogenesis. Rev. Mineral. Geochem. 53 (1), 27–62.

Hou, Z.Q, Duan, L.F, Lu, Y.J, Zheng, Y.C, Zhu, D.C., Yang, Z.M., Yang, Z.S., Wang, B.D., Pei, Y.R., Zhao, Z.D., Mccuaig, T.C., 2015. Lithospheric architecture of the Lhasa terrane and its control on ore deposits in the Himalayan-Tibetan orogen. Econ. Geol. 110, 1541–1575.

Hu, D.G., Wu, Z.H., Jiang, W., Shi, Y.R., Ye, P.S., Liu, Q.S., 2005. SHRIMP zircon U–Pb age and Nd isotopic study on the Nyainqêntanglha Group in Tibet. Sci. China 48 (9), 1377–1386.

Hu, P.Y, Li, C., Wang, M., Xie, C.M, Wu, Y.W., 2013. Cambrian volcanism in the Lhasa terrane, southern Tibet: Record of an early Paleozoic Andean-type magmatic arc along the Gondwana proto-Tethyan margin. J. Asian Earth Sci. 77, 91–107.

Hu, P.Y., Zhai, Q.G., Wang, J., Tang, Y., Wang, H.T., Zhu, Z.C., W, H., 2018a. Middle Neoproterozoic (~ 760 Ma) arc and back-arc system in the North Lhasa terrane, Tibet, inferred from coeval N-MORB- and arc-type gabbros. Precambrian Res. 316, 275–290.

Hu, P.Y., Zhai, Q.G., Wang, J., Tang, Y., Wang, H.T., Hou, K.J., 2018b. Precambrian origin of the north Lhasa terrane, Tibetan Plateau: Constraint from early Cryogenian back-arc magmatism. Precambrian Res. 313, 51–67.

Ji, W.Q., Wu, F.Y., Chung, S.L., Li, J.X., Liu, C.Z., 2009. Zircon U–Pb geochronology and Hf isotopic constraints on petrogenesis of the Gangdese batholith, southern Tibet. Chem. Geol. 262, 229–245.

Ji, W.Q., Wu, F.Y., Chung, S.L., Liu, C.Z., 2012. Identification of early Carboniferous granitoids from southern Tibet and implications for terrane assembly related to the Paleo-Tethyan evolution. J. Geol. 120 (5), 531–541.

Ji, W.Q., Wu, F.Y., Liu, C.Z., Zhang, H., 2017. Zircon U–Pb geochronology and Hf isotopes of granitic rocks and river sands in the Nyingchi region, Tibet: Constraints on evolution of the deep crust beneath the southeast Lhasa terrane. J. Asian Earth Sci. 145, 613–625.

Kang, D.Y., Zhang, Z.M., Dong, X., Tian, Z.L., Xiang, H., Mo, X.X., 2019. Anticlockwise *P-T-t* path and tectonic mechanism of metapelites from the eastern Gangdese arc, southern Tibet. Acta Petrol. Sin. 35 (2), 349–362 (in Chinese with English abstract).

Keto, L.S., Jacobsen, S.B., 1987. Nd and Sr isotopic variations of Early Paleozoic ocean. Earth Planet. Sci. Lett. 84 (1), 27–41.

Kidd, W.F., Pan, Y.S., Chang, C.F., Coward, M.P., Dewey, J.F., Gansser, A., Molnar, P., Shackleton, R.M., Sun, Y.J., 1988. Geological mapping of the 1985 Chinese–British Tibetan (Xizang–Qinghai) Plateau geotraverse route. Phil. Trans. Roy. Soc. Lond. A 327, 287–305.

Kröner, A., Santosh, M., Wong, J., 2012. Zircon ages and Hf isotopic systematics reveal vestiges of Mesoproterozoic to Archaean crust within the late

Neoproterozoic-Cambrian high-grade terrain of southernmost India. Gondwana Res. 21 (4), 876–886.

Leake, B.E., et al., 1997. Nomenclature of amphiboles: Report of the subcommittee on amphiboles of the International Mineralogical Association. Commission on New Minerals and Mineral Names. Mineral. Mag. 35, 219–246.

Leier, A.L., Kapp, P., Gehrels, G.E., DeCelles, P.G., 2007. Detrital zircon geochronology of Carboniferous-Cretaceous strata in the Lhasa terrane, southern Tibet. Basin Res. 19 (3), 361–378.

Li, G.W., Sandiford, M., Liu, X.H., Xu, Z.Q., Wei, L.J., Li, H.Q., 2014. Provenance of Late Triassic sediments in central Lhasa terrane, Tibet and its implication. Gondwana Res. 25 (4), 1680–1689.

Li, P., 1955. Primary understanding of geology, eastern Tibet. Chin. Sci. Bull. 7 (7), 62–71 (in Chinese).

Lin, Y.H., Zhang, Z.M., Dong, X., Xiang, H., Yan, R., 2013a, Early Mesozoic metamorphism and tectonic significance of the eastern segment of the Lhasa terrane, south Tibet. J. Asian Earth Sci. 78, 160–183.

Lin, Y.H., Zhang, Z.M., Dong, X., Shen, K., Lu, X., 2013b. Precambrian evolution of the Lhasa terrane, Tibet: Constraint from the zircon U–Pb geochronology of the gneisses. Precambrian Res. 237, 64–77.

Maniar, P.D., Piccoli, P.M., 1989. Tectonic discrimination of granitoids. Geol. Soc. Am. Bull. 101 (5), 635–643.

McWilliams, M.O., 1981. Palaeomagnetism and Precambrian tectonic evolution of

Gondwana. In: Kro¨ner, A. (Ed.), Precambrian Plate Tectonics. Elsevier, Amsterdam, pp. 649–687.

Meert, J.G., Van der Voo, R., Ayub, S., 1995. Paleomagnetic investigation of the Neoproterozoic Gagwe lavas and Mbozi complex, Tanzania and the assembly of Gondwana. Precambrian Res. 74 (4), 225–244.

Meert, J.G., Van der Voo, R., 1997. The assembly of Gondwana 800–550 Ma. J. Geodyn. 23 (3–4), 223–235.

Meert, J.G., 2001. Growing Gondwana and rethinking Rodinia: A paleomagnetic perspective. Gondwana Res. 4 (3), 279–288.

Meert, J.G., 2003. A synopsis of events related to the assembly of eastern Gondwana. Tectonphysics 362, 1–40.

Meert, J.G., Torsvik, T.H., 2003. The making and unmaking of a supercontinent: Rodinia revisted. Tectonophysics 375, 261–288.

Meng, Y.K., Dong, H.W., Cong, Y., Xu, Z.Q., Cao, H., 2016. The early-stage evolution of the Neo-Tethys ocean: Evidence from granitoids in the middle Gangdese batholith, southern Tibet. J. Geodyn. 94–95, 34–49.

Mo, X.X., Hou, Z.Q., Niu, Y.L., Dong, G.C., Qu, X.M., Zhao, Z.D., Yang, Z.M., 2007. Mantle contributions to crustal thickening during continental collision: Evidence from Cenozoic igneous rocks in southern Tibet. Lithos 96 (1–2), 225–242.

Mukherjee, A., Das, S., 2002. Anorthosites, Granulites and the Supercontinent Cycle. Gondwana Res. 5 (1), 147–156.

Nijland, T.G., Maijer, C., 1993. The regional amphibolite to granulite facies transition at Arendal, Norway: Evidence for a thermal dome. N. Jahrb. Mineral. Abh. 165, 191–221.

Nijland, T.G., Visser, D., 1995. Provenance of the Bamble amphibolites, Norway. Proc. R. Neth. Acad. Arts Sci. 98 (1–2), 69–88.

Nimaciren, Xie, Y.W., Sha, Z.L., Xiluolangjie, Qiangbazaxi, Peng, D.P., Gesangsuolang, Luosongzhandui, 2005. 1: 250, 000 geological report of Nagqu County with geological map. Xizang Institute of Geological Survey, Lhasa, 103–107 (in Chinese).

Palin, R.M., Searle, M.P., St-Onge, M.R., Waters, D.J., Roberts, N.M.W., Horstwood, M.S.A., Parrish, R.R., Weller, O.M., Chen, S., Yang, J., 2014. Monazite geochronology and petrology of kyanite- and sillimanite-grade migmatites from the northwestern flank of the eastern Himalayan syntaxis. Gondwana Res. 26 (1), 323–347.

Palin, R.M., White, R.W., Green, E.C.R., Diener, J.F.A., Powell, R., Holland, T.J.B., 2016. High-grade metamorphism and partial melting of basic and intermediate rocks. J. Metamorph. Geol. 34, 871–892.

Pan, G.T., Ding, J., Yao, D.S., Wang, L.Q., 2004. Guidebook of 1:1,500,000 geologic map of the Qinghai–Xizang (Tibet) plateau and adjacent areas. Cartographic Publishing House, Chengdu, China, pp. 1–148 (in Chinese).

Pan, G.T., Mo, X.X., Hou, Z.Q., Zhu, D.C., Wang, L.Q., Li, G.M., Zhao, Z.D., Geng, Q.R., Liao, Z.L., 2006. Spatial-temporal framework of the Gangdese Orogenic

Belt and its evolution. Acta Petrol. Sin. 22 (3), 521–533 (in Chinese with English abstract).

Piper, J.D.A., 1976. Palaeomagnetic evidence for a Proterozoic super-continent. Phil. Trans. Roy. Soc. Lond. A 280, 469–490.

Pullen, A., Kapp, P., Gehrels, G.E., DeCelles, P.G., Brown, E.H., Fabijanic, J.M., Ding, L., 2008. Gangdese retroarc thrust belt and foreland basin deposits in the Damxung area, southern Tibet. J. Asian Earth Sci. 33 (5–6), 323–336.

Rogers, J.J.W., Santosh, M., 2002. Configuration of Columbia, a Mesoproterozoic Supercontinent. Gondwana Res. 5 (1), 5–22.

Rollinson, H., 1993. Using Geochemical Data: Evaluation, Pre-sentation, Interpretation. Longman, London. 215–263 pp.

Rubatto, D., Hermann, J., Berger, A., Engi, M., 2009. Protracted fluid-induced melting during barrovian metamorphism in the central Alps. Contrib. Mineral. Petrol. 158 (6), 703–722.

Rubatto, D., 2017. Zircon: The Metamorphic Mineral. Rev. Mineral. Geochem. 83, 261–296.

Sadowski, G.R., Bettencourt, J.S., 1996. Mesoproterozoic tectonic correlations between eastern Laurentia and the western border of the Amazon Craton. Precambrian Res. 76 (3–4), 213–227.

Sawyer, E.W., 2001. Melt segregation in the continental crust: Distribution and movement of melt in anatectic rocks. J. Metamorph. Geol. 19 (3), 291–309.

Sengör, A.M.C., Natal'in, B.A., 1996. Paleotectonics of Asia: Fragments of a synthesis. In: Yin, A., Harrison, M.T. (Eds.), The Tectonic Evolution of Asia, Cambridge University Press, pp. 486–640.

Silveira, E.M., Söderlund, U., Oliveira, E.P., Ernst, R.E., Menezes Leal, A.B., 2013. First precise U–Pb baddeleyite ages of 1500 Ma mafic dykes from the São Francisco Craton, Brazil, and tectonic implications. Lithos 174, 144–156.

Sun, S.S., McDonough, W.F., 1989. Chemical and isotope systematics of oceanic basalts: Implications for mantle composition and processes. In: Saunders, A.D. (Ed.), Magmatism in Ocean Basins. Geological Society of London Special Publication, pp. 313–345.

Timmermann, H., Jamieson, R.A., Parrish, R.R., Culshaw, N.G., 2002. Coeval migmatitues and granulites, Muskoka domain, southwestern Grenville Province, Ontano. Can. J. Earth Sci. 39 (2), 239–258.

Veevers, J.J., 2004. Gondwanaland from 650–500 Ma assembly through 320 Ma merger in Pangea to 185–100 Ma breakup: Supercontinental tectonics via stratigraphy and radiometric dating. Earth Sci. Rev. 68, 1–132

Weis, D., 1986. Genetic implications of Pb isotopic geochemistry in the Rogaland anorthositic complex (southwest Norway). Chem. Geol. 57 (1), 181–199.

Weller, O.M., St-Onge, M.R., Searle, M.P., Waters, D.J., Rayner, N., Chen, S., Chung, S.L., Palin, R.M., 2015. Quantifying the *P–T–t* conditions of north–south Lhasa terrane accretion: New insight into the pre-Himalayan architecture of the Tibetan plateau. J. Metamorph. Geol. 33 (1), 91–113.

Xie, C.M., Li, C., Su, L., Wu, Y.W., Wang, M., Yu, H., 2010. LA–ICP–MS U–Pb dating of zircon from granite–gneiss in the Amdo area, northern Tibert, China. Geolo. Bull. Chin. 29 (12), 1737–1744 (in Chinese with English abstract).

Xie, R.W., Peng, X.J., Xiluelangjie, Bao, J.Y., Duan, G.X., He, C.H., Qiangbazhax, Sha, S.L., Chen, Y.M., Chen, D.Q., Peng, D.P., 2007. 1:250, 000 geological report of Zêtang Town with geological map. Geological Survey of Tibet Autonomous Region Press, Lhasa, pp. 1–315 (in Chinese).

Xu, R.H., Schärer, U., Allègre, C.J., 1985. Magmatism and metamorphism in the Lhasa block (Tibet): A geochronological study. J. Geol. 93(1), 41–57.

Xu, W.C., Zhang, H.F., Harris, N., Guo, L., Pan, F.B., Wang, S., 2013a. Geochronology and geochemistry of Mesoproterozoic granitoids in the Lhasa terrane, south Tibet: Implications for the early evolution of Lhasa terrane. Precambrian Res. 236, 46–58.

Xu, W.C., Zhang, H.F., Harris, N., Guo, L., Pan, F.B., 2013b. Rapid Eocene erosion, sedimentation and burial in the eastern Himalayan syntaxis and its geodynamic significance. Gondwana Res. 23 (2), 715–725.

Yang, J.S., Xu, Z.Q., Li, Z.L., Xu, X.Z., Li, T.F., Ren, Y.F., Li, H.Q., Chen, S.Y., Robinson, P.T., 2009. Discovery of an eclogite belt in the Lhasa block, Tibet: A new border for Paleo-Tethys? J. Asian Earth Sci. 34 (1), 76–89.

Yang, Z.M., Hou, Z.Q., Jiang, Y.F., Zhang, H.R., Song, Y.C., 2011. Sr-Nd-Pb and zircon Hf isotopic constraints on petrogenesis of the Late Jurassic granitic porphyry at Qulong, Tibet. Acta Petrol. Sin. 27 (7), 2003–2010 (in Chinese with English abstract).

Yin, A., Harrison, T.M., 2000. Geologic evolution of the Himalayan–Tibetan orogen. Annu. Rev. Earth Planet. Sci. 28, 211–280.

Yin, A., Nie, S., 1996. A Phanerozoic palinspastic reconstruction of China and its neighboring regions. In: Yin, A., Harrison, M.T. (Eds.), The Tectonic Evolution of Asia. Cambridge University Press, pp. 442–485.

Yin, G.G., Chen, Y.P., Su, X.J., Bao, J.Y., Hou, S.Y., Lu, Y., Duan, G.X., Zhang, J.Y., Liu, Z., Xiao, L., 2003. 1:250,000 geological report of Nyingtri region with geological map. Yunnan, Institute of Yunnan Geological Survey (in Chinese).

Zeng, L.S., Liu, J., Gao, L.E., Chen, F.Y., Xie, K.J., 2009. Early Mesozoic high-pressure metamorphism within the Lhasa block, Tibet and implications for regional tectonics. Earth Sci. Front. 16 (2), 140–151.

Zeng, Y.C., Chen, Q, Xu, J.F., Chen, J.L., Huang, F., Yu, H.X., Zhao, P.P., 2018. Petrogenesis and geodynamic significance of neoproterozoic (~ 925 Ma) high-Fe-Ti gabbros of the Rentso ophiolite, Lhasa terrane, central Tibet. Precambrian Res. 314, 160–169.

Zhang, H.F., Xu, W.C., Guo, J.Q., Zong, K.Q., Cai, H.M., Yuan, H.L., 2007a. Zircon U–Pb and Hf isotopic composition of deformed granite in the southern margin of the Gangdese Belt, Tibet: Evidence for early Jurassic subduction of Neo-Tethyan oceanic slab. Acta Petrol. Sin. 23 (6), 1347–1353 (in Chinese with English abstract).

Zhang, H.F., Xu, W.C., Guo, J.Q., Zong, K.Q., Cai, H.M., Yuan, H.L., 2007b. Indosinian orogenesis of the Gangdese terrane: Evidences from zircon U–Pb dating and petrogenesis of granitoids. Earth Sci. J. China Univ. Geosci. 32 (2), 155–166 (in Chinese with English abstract).

Zhang, K.J., Zhang, Y.X., Li, B., Zhong, L.F., 2007. Nd isotopes of siliciclastic rocks from Tibet, western China: Constraints on provenance and pre-Cenozoic tectonic evolution. Earth Planet. Sci. Lett. 256 (3–4), 604–616.

Zhang, X.R., Shi, R.D., Huang, Q.S., Liu, D.L., Gong, X.H., Chen, S.S., Wu, K., Yi, G.D., Sun, Y.L., Ding, L., 2014. Early Jurassic high-pressure metamorphism of the Amdo terrane, Tibet: Constraints from zircon U-Pb geochronology of mafic granulites. Gondwana Res. 26 (3–4), 975–985.

Zhang, Z.M., Zhao, G.C., Santosh, M., Wang, J.L., Dong, X., Liou, J.G., 2010. Two stages of granulite facies metamorphism in the eastern Himalayan syntaxis, south Tibet: Petrology, zircon geochronology and implications for the subduction of Neo-Tethys and the Indian continent beneath Asia. J. Metamorph. Geol. 28 (7), 719–733.

Zhang, Z.M., Dong, X., Liu, F., Lin, Y.H., Yan, R., Santosh, M., 2012a. Tectonic evolution of the Amdo terrane, central Tibet: Petrochemistry and zircon U–Pb geochronology. J. Geol. 120 (4), 431–451.

Zhang, Z.M., Dong, X., Liu, F., Lin, Y.H., Yan, R., He, Z.Y., Santosh, M., 2012b. The making of Gondwana: Discovery of 650 Ma HP granulites from the North Lhasa, Tibet. Precambrian Res. 212–213, 107–116.

Zhang, Z.M., Dong, X., Xiang, H., Liou, J.G., Santosh, M., 2013. Building of the deep Gangdese arc, South Tibet: Paleocene plutonism and granulite-facies metamorphism. J. Petrol. 54 (12), 2547–2580.

Zhang, Z.M., Dong, X., Santosh, M., Zhao, G.C., 2014a. Metamorphism and tectonic evolution of the Lhasa terrane, Central Tibet. Gondwana Res. 25 (1), 170–189.

Zhang, Z.M., Dong, X., Xiang, H., He, Z.Y., Liou, J.G., 2014b. Metagabbros of the Gangdese arc root, south Tibet: Implications for the growth of continental crust Geochim. Cosmochim. Acta 143, 268–284.

Zhang, Z.M., Dong, X., Xiang, H., Ding, H.X., He, Z.Y., Liou, J.G., 2015. Reworking of the Gangdese magmatic arc, southeastern Tibet: Post-collisional metamorphism and anatexis. J. Metamorph. Geol. 33 (1), 1–21.

Zhao, G.C., Sun, M., Wilde, S.A., Li, S.Z., 2003. Assembly, accretion, and break-up of the Palaeo-Mesoproterozoic Columbia supercontinent: Record in the North China Craton revisited. Gondwana Res. 6 (3), 417–434.

Zhu, D.C., Pan, G.T., Chung, S.L., Liao, Z.L., Wang, L.Q., Li, G.M., 2008. SHRIMP zircon age and geochemical constraints on the origin of lower Jurassic volcanic rocks from the Yeba formation, southern Gangdese, south Tibet. Int. Geol. Rev. 50 (5), 442–471.

Zhu, D.C., Mo, X.X., Niu, Y., Zhao, Z.D., Wang, L.Q., Liu, Y.S., Wu, F.Y., 2009a. Geochemical investigation of Early Cretaceous igneous rocks along an east–west traverse throughout the central Lhasa Terrane, Tibet. Chem. Geol. 268 (3–4), 298–312.

Zhu, D.C., Mo, X.X., Niu, Y.L., Zhao, Z.D., Wang, L.Q., Pan, G.T., Wu, F.Y., 2009b. Zircon U–Pb dating and in-situ Hf isotopic analysis of Permian peraluminous granite in the Lhasa terrane, southern Tibet: Implications for Permian collisional orogeny and paleogeography. Tectonophysics 469 (1–4), 48–60.

Zhu, D.C., Zhao, Z.D., Niu, Y.L., Mo, X.X., Chung, S.L., Hou, Z.Q., Wang, L.Q., Wu, F.Y., 2011. The Lhasa Terrane: Record of a microcontinent and its histories of drift and growth. Earth Planet. Sci. Lett. 301 (1–2), 241–255.

Zhu, D.C., Zhao, Z.D., Niu, Y.L., Dilek, Y., Wang, Q., Ji, W.H., Dong, G.C., Sui, Q.L., Liu, Y.S., Yuan, H.L., Mo, X.X., 2012. Cambrian bimodal volcanism in the Lhasa Terrane, southern Tibet: Record of an early Paleozoic Andean-type magmatic arc in the Australian proto-Tethyan margin. Chem. Geol. 328, 290–308.

Zhu, D.C., Zhao, Z.D., Niu, Y., Dilek, Y., Hou, Z.Q., Mo, X.X., 2013. The origin and pre-Cenozoic evolution of the tibetan plateau. Gondwana Res. 23 (4), 1429–1454.

Figure captions:

Figure 1. (a) Tectonic framework of the Tibetan Plateau (after Zhu et al., 2013), showing the major tectonic subdivisions. NLT = Northern Lhasa subterrane, CLT = Central Lhasa subterrane, SLT = Southern Lhasa subterrane, JSSZ = Jinsha Suture Zone, LSSZ = Longmu Tso-Shuanghu Suture Zone, BNSZ = Bangong-Nujiang Suture Zone, SNMZ = Shiquan River-Nam Tso M~~m~~élange Zone~~zone~~, LMF = Luobadui-Milashan Fault, IYZSZ = Indus-Yarlung Zangbo Suture Zone. Data sources

of the Precambrian magmatic rocks for Amdo: ~ 820 Ma and 500 Ma (Zhang et al., 2012a), 852 Ma (Guynn et al., 2006), 532 Ma (Guynn et al., 2012); the CLT from west to east: 492 Ma (Zhu et al., 2012), 525–510 Ma (Hu et al., 2013), 512 Ma (Ding et al., 2015), 787 Ma (Hu et al., 2005), 897–886 Ma (Zhang et al., 2012b), 760 Ma (Hu et al., 2018a), 822–806 Ma (Hu et al., 2018b), 925 Ma (Zeng et al., 2018), 1343– ~~Ma and~~ 1250 Ma (Xu et al., 2013a; Chen et al., 2019), 1866 Ma (Chen et al., 2019); the SLT: 496 Ma (Dong et al., 2010). (b) Geological sketch map of the Dongjiu area in the SLT, the Paleoproterozoic data (~ 1780 Ma) from Lin et al. (2013b).~~.~~

Figure 2. ~~Field photographs of Dongjiu gneiss. (a) Outcrop of the Dongjiu gneiss. (b) Closeup photo showing banded structure with millimeter-size white leucosome.Figure 3.~~ Photomicrographs of representative Dongjiu gneiss. (a) Biotite (Bt)- amphibole (Amp~~amp~~) gneiss, consisting of amphibole, plagioclase (Pl), K-feldspar (Kfs), biotite, quartz (Qz) and titanite (Ttn) riming ilmenite (Ilm), with minor apatite (Ap). (b) Bt-amp gneiss, showing plagioclase with cuspate extensions along quartz-quartz contacts. (c) and (d) Bt-amp gneiss, showing allanite (Aln) replaced by epidote (Ep) in rim, with zircon (Zrn) inclusions. (e) Bt gneiss, consisting of plagioclase, K-feldspar, biotite, quartz, with minor allanite replaced by epidote at rim; adjacent grains of quartz, plagioclase and K-feldspar~~ grains~~ are corroded. (f) Bt gneiss, showing adjacent plagioclase and biotite grains are corroded; narrow K-feldspar blebs at quartz-plagioclase contacts.

Figure 34. (a) Ab-An-Or classification for silicic rocks from Barker (1979). (b) A/CNK vs A/NK diagram from Maniar and Piccoli (1989). The data of the Bomi Mesoproterozoic granitoids are after Xu et al. (2013a).

Figure 4.~~5.~~ (a) Chondrite-normalized REE and (b) Primitive-mantle-normalized trace element patterns for the Dongjiu gneiss. The data of the Bomi Mesoproterozoic granitoids are after Xu et al. (2013a). The normalization data are from Sun and McDonough (1989).

Figure 5.~~6.~~ Zircon U–Pb concordia diagrams and chondrite-normalized REE patterns of the Dongjiu Bt-amp gneiss. (a), (c) and (e) Zircon U–Pb concordia diagrams, red and blue elliptises represent zircon core and rim ages, respectively. (b), (d) and (f) Chondrite-normalized REE patterns, showing CL images of representative zircon grains. Red and blue circles indicate zircon core and rim dating spots with ages in Ma, respectively. The normalization data are from Sun and McDonough (1989).

Figure 6.~~7.~~ Zircon U–Pb concordia diagrams and chondrite-normalized REE patterns of the Dongjiu Bt gneiss.~~gneisses.~~ (a) and (c) Zircon U–Pb concordia diagrams, red and blue ellipses represent zircon core and rim ages, respectively. (b) and (d) Chondrite-normalized REE patterns, showing CL images of representative zircon grains. Red and blue circles indicate zircon core and rim ages with ages in Ma, respectively. The normalization data are from Sun and McDonough (1989).

Figure 7~~8~~. BSE images and photomicrographs of representative titanite for the Dongjiu Bt-amp gneiss. Representative titanite (a)–(h) for sample 169-1, (i)–(p) for sample 39-1. (a)–(d) and (i)–(l) Blue circles are spots for dating with ^{207}Pb corrected $^{206}Pb/^{238}U$ ages in Ma. (e)–(h) and (m)–(p) Most titanite including ilmenite, biotite, allanite, apatite, plagioclase, quartz and minor~~miner~~ rutile.

Figure 8~~9~~. Titanite U–Pb concordia diagrams of the Dongjiu Bt-amp gneiss.

Figure 9~~10~~. Frequency histogram of Zr-in-titanite temperatures for the Dongjiu Bt-amp gneiss.

Figure 10. Zircon U vs Th contents diagram of the Dongjiu gneiss.

Figure 11. Zircon U~~ vs Th diagram.Figure 12. Zircon U~~-Pb age vs $\varepsilon_{Hf}(t)$ diagram for the Dongjiu gneiss and related rocks~~samples~~ from the Lhasa terrane. Data sources: SLT ~ 1500 Ma gneiss (our unpublished data); SLT granitoids (Chu et al., 2006; Zhang et al., 2007a; Ji et al., 2009, 2012; Yang et al., 2011; Zhu et al. 2011; Dong et al., 2013, 2014, 2015; Guo et al., 2013; Meng et al., 2016); CLT granitoids (Zhang et al., 2007b; Zhu et al., 2009b, 2011, 2012; Xu et al., 2013a; Hu et al., 2018b; Chen et al., 2019); SLT Paleozoic strata (Guo et al., 2017); CLT Paleozoic strata (Zhu et al., 2013; Li et al., 2014).

HIGHLIGHTS

The Mesoproterozoic rocks (1520–1506 Ma) are recognized in the southern Lhasa subterrane (SLT).

Bulk-rock Nd and zircon Hf isotopes show their derivation from the Paleoproterozoic material.

The Mesoproterozoic rocks metamorphosed at 605–590 Ma represent the Precambrian metamorphic basement of the Lhasa terrane.

Titanite *in situ* U-Pb dating gives more recent metamorphic age of ~ 26 Ma.

The SLT basement has been strongly reworked by mantle-derived magmatism and metamorphism since the Mesozoic.

Reworked Precambrian metamorphic basement of the Lhasa terrane, southern Tibet: Zircon/Titanite U–Pb geochronology, Hf isotope and Geochemistry

Dong Xin[1, 2], Zhang Zeming[1], Niu Yaoling[2], Tian Zuolin[1], Zhang Liangliang[3]

1. Key Laboratory of Deep-Earth Dynamics of Ministry of Land and Resources, Institute of Geology, Chinese Academy of Geological Sciences, Beijing, 100037, China
2. Department of Earth Sciences, Durham University, Durham, DH1 3LE, UK
3. State Key Laboratory of Geological Processes and Mineral Resources, and Institute of Earth Sciences, China University of Geosciences, Beijing, 100083, China

ABSTRACT

Due to the paucity of exposure, the formation and evolution of the Precambrian basement of the Lhasa terrane remain poorly known. Here we report zircon and titanite *in situ* U–Pb ages, bulk-rock geochemical and zircon Hf isotopic data on the orthogneisses from the Dongjiu area of the southern Lhasa subterrane (SLT), southern Tibet. Geochemical data suggest that the protoliths of the biotite-amphibole gneiss and biotite gneiss are granodiorite and granite, respectively. Inherited magmatic zircon cores from these orthogneisses give protolith crystalline ages of 1520–1506 Ma, whereas the overgrown zircon rims give metamorphic ages of 605–590 Ma. The

Mesoproterozoic granitic rocks have bulk-rock $\varepsilon_{Nd}(t)$ values of -3.6 to +0.1 and zircon core $\varepsilon_{Hf}(t)$ values of -4.5 to +2.6, which give similar T_{DM2} ages of 2.35–2.05 Ga and 2.54–2.10 Ga respectively, suggesting their derivation from partial melting of Paleoproterozoic crustal material. The granitic rocks are also local provenance for the Mesoproterozoic detrital zircons in the Paleozoic strata in the Lhasa terrane. Titanite *in situ* U–Pb ages further indicate that the Dongjiu orthogneiss experienced more recent metamorphism at ~ 26 Ma. The mineral assemblage and thermobarometry calculations indicate that the Oligocene metamorphism occurred under medium-pressure (MP) amphibolite-facies conditions (5.4–7.2 kbar, 691–765 °C). We propose that the Dongjiu gneisses represent the Precambrian metamorphic basement of the Lhasa terrane, but have been intensively reworked by metamorphism in the SLT in response to the continued India-Asia convergence since the collision.

Keywords:

Zircon and Titanite *in situ* U–Pb dating; Mesoproterozoic; Precambrian metamorphic basement; Reworking; Lhasa terrane

1. Introduction

Like much of the central and southeastern Asian geology, the Tibetan Plateau formed via amalgamation of terranes during the Phanerozoic (Chang and Zheng, 1973; Allégre et al., 1984; Chang et al., 1986; Sengör and Natal'in, 1996; Yin and

Nie, 1996). However, our knowledge on the histories of these terranes prior to their amalgamation remains limited. The early history of these terranes that make up the Tibetan Plateau is obscured by the paucity of basement exposure, by the strong reworking of basement rocks during the later thermal events, and by the predominance of younger supracrustal rocks.

As the main tectonic component of the Tibetan Plateau, the Lhasa terrane has been considered to be composed dominantly of Paleozoic to Mesozoic strata, Mesozoic and Cenozoic igneous rocks and Precambrian basement (e.g., Yin and Harrison, 2000; Pan et al., 2004, 2006). The nature and spatial distribution of the Precambrian basement beneath the entire terrane have been speculative. The limited works on the basement to date suggest that the Lhasa terrane crust is relatively young (< 2.0 Ga). U–Pb dating of zircons in gneissic rocks shows the presence of the Neoproterozoic crystalline crust in the Amdo block (~ 850 Ma, Guynn et al., 2006, 2012; Zhang et al., 2012a) and in the Xainza area in the central Lhasa subterrane (CLT) (~ 925–760 Ma, Hu et al., 2005; Zhang et al., 2012b; Hu et al., 2018a, b; Zeng et al., 2018). There is also Proterozoic crystalline basement in the Bomi area in the eastern CLT (ca. 1866 Ma, 1343–1250 Ma and 824 Ma, Xu et al., 2013a; Chen et al., 2019) (Fig. 1a). These ages represent the only known Precambrian crystalline basement from the Lhasa terrane. Nd-Hf isotopic model ages have been used to suggest that the crust of the Lhasa terrane may be older, perhaps even Archean. Bulk-rock Nd isotope data on the Amdo Cambrian orthogneiss give Mesoproterozoic model ages (Harris et al., 1988a), while bulk-rock Nd and zircon Hf isotopic data on the

Cretaceous granitoids of the Lhasa terrane yield Proterozoic and Archean model ages (Chiu et al., 2009; Zhu et al., 2009a). Zhu et al. (2011) suggest that the CLT was once a microcontinent with Proterozoic and Archean basement rocks, whereas the southern and northern parts of the Lhasa terrane are dominated by younger juvenile crust. However, zircon Hf isotopic mapping for the Mesozoic-Cenozoic magmatic rocks shows that the eastern segment of the northern Lhasa subterrane (NLT) is an ancient block; the southern Lhasa subterrane (SLT) is not entirely a juvenile block with inhomogeneity of crustal compositions (Hou et al., 2015). However, no Archean rocks have been identified so far. It is possible that the enriched radiogenic isotopic compositions could have resulted from the assimilation of melted sedimentary rocks that were themselves sourced from older continents (e.g., Indian craton), rather than from pre-Neoproterozoic basement of the Lhasa terrane itself (Ding et al., 2003). Therefore, the true and complete constituent of the Precambrian basement beneath the Lhasa terrane remains to be revealed.

In this paper, we report the results of petrological, geochronological and geochemical studies on reworked Precambrian metamorphic basement rocks from the Dongjiu area of the SLT (Fig. 1). The metamorphic rocks not only provide information on their protolith, but also record two episodes of subsequent metamorphism and Phanerozoic reworking of the Precambrian basement of the Lhasa terrane.

2. Geological setting and sample description

2.1. Geological setting

The Lhasa terrane on the southern segment of the Tibetan Plateau is located between the Qiangtang terrane and Himalayan belt, bounded by the Bangong-Nujiang suture zone to the north and the Indus-Yarlung Zangbo suture zone to the south (Fig. 1a). From north to south, the Lhasa terrane has been divided into the northern, central and southern subterranes, separated by the Shiquan River-Nam Tso mélange zone to the north and the Luobadui-Milashan fault to the south (Fig. 1a; Zhu et al., 2009a).

The NLT is characterized by the presence of juvenile crust and absence of a Precambrian basement (cf. Pan et al., 2004; Zhu et al., 2011). The sedimentary cover in the NLT is mainly Jurassic–Cretaceous with minor Triassic in age (e.g., Pan et al., 2004, 2006; Nimaciren et al., 2005). Voluminous Mesozoic volcanic rocks are exposed in this subterrane, and Mesozoic plutonic rocks are mainly confined to its western and eastern segments generally as huge batholiths (e.g., Zhu et al., 2011).

The CLT is covered with the widespread Permo-Carboniferous metasedimentary rocks, plus minor Ordovician, Silurian and Triassic strata (cf. Pan et al., 2004). The volcanic rocks in this subterrane are mostly early Cretaceous in age with minor being Permian. The Mesozoic plutonic rocks occur as batholiths of varying age (~ 215–88 Ma; cf. Zhu et al., 2011 and references therein). Cambrian volcanic rocks are scattered in the west and middle of the CLT (Fig. 1a, Zhu et al., 2012; Hu et al., 2013; Ding et al., 2015). The late Permian high-pressure eclogite and late Triassic–early

Jurassic metamorphic rocks are exposed in the middle and eastern parts of the CLT (e.g., Yang et al., 2009; Zeng et al., 2009; Dong et al., 2011a; Lin et al., 2013a; Cheng et al., 2015; Weller et al., 2015; Chen et al., 2017). The Nyainqêntanglha Group in the middle part of the CLT has been interpreted as its Precambrian basement (Li, 1955; Allégre et al., 1984; Harris et al., 1988b; Pan et al., 2004). On the basis of zircon U–Pb dating, the protoliths of the Nyainqêntanglha Group near Xainza area were emplaced in the Neoproterozoic (Fig. 1a, Hu et al., 2005; Zhang et al., 2012b; Hu et al., 2018a, b; Zeng et al., 2018). Recent petrological studies with zircon U–Pb age data reveal that the rocks from the Xainza area are the relics of the Neoproterozoic (~ 900 Ma) ocean crust metamorphosed subsequently at ~ 690–650 Ma (Dong et al., 2011b; Zhang et al., 2012b). Moreover, Xu and co-workers (Xu et al., 2013a; Chen et al., 2019) reported the presence of Proterozoic basement with crystallization ages of ca. 1866 Ma, 1343–1250 Ma and 824 Ma from the Bomi complex in the southeastern CLT. Chen et al. (2019) suggested that these Proterozoic gneisses revealed two metamorphic events at ca. 625–600 Ma and 80 Ma. These new data confirm the presence of a Precambrian metamorphic basement in the CLT.

The SLT is mainly composed of the Paleogene volcanic rocks, Cretaceous–Tertiary intrusions, Triassic–Cretaceous volcano-sedimentary rocks and minor medium- to high-grade metamorphic rocks (e.g., Pan et al., 2004; Zhu et al., 2008, 2013; Zhang et al., 2014a). The sedimentary cover in the SLT is largely restricted to its eastern segment (cf. Pan et al., 2004). The Nyingchi complex in the eastern SLT has been interpreted as the Precambrian basement (Pan et al., 2004; Yin et al., 2003;

Xie et al., 2007). However, more recent studies indicated that most protoliths of the Nyingchi complex included both sedimentary and magmatic rocks of Cambrian (~ 496 Ma), Devonian (~ 360 Ma), Cretaceous (~ 90 Ma) and Eocene (~ 55 Ma), metamorphosed in the Mesozoic to Cenozoic (Dong et al., 2010, 2012, 2014; Guo et al., 2011, 2012; Palin et al., 2014; Xu et al., 2013b; Zhang et al., 2010, 2013, 2014a, b, 2015). Based on zircon U–Pb dating, Lin et al. (2013b) reported a metamorphic age of ~ 600 Ma from the Nyingchi complex in the eastern SLT, with a protolith age of ~ 1780 Ma. However, their samples are close to the northeast of the Eastern Himalayan Syntaxis, and are widely intruded by the Mesozoic–Cenozoic granitoids or occur as xenoliths within these granitoids (Lin et al., 2013b). Therefore, a Precambrian crystalline basement may indeed be present at least locally in the SLT.

The present study area is located northwest of the Dongjiu area at the eastern edge of the SLT, where metamorphic rocks and Cenozoic intrusive rocks are exposed (Fig. 1b). The metamorphic rocks are offset by an east-west fault. The rocks north of the fault include schists and gneisses that experienced amphibolite-facies metamorphism at ~ 190 Ma (Chen et al., 2017). The studied samples are gneisses collected south of the fault. These metamorphic rocks are all intruded by the Cenozoic granites (~ 40–25 Ma; Booth et al., 2004).

2.2. Sample description

Sample details are given in Table 1, including protolith type, location, mineral assemblage, protolith and metamorphic ages, and metamorphic *P*–*T* conditions.

The biotite-amphibole (Bt-amp) gneisses consist of plagioclase (~30 vol%), K-feldspar (~15 vol%), quartz (~35 vol%), amphibole (~10 vol%), biotite (~5 vol%), titanite (~3 vol%), allanite (~1 vol%), and accessory phases including epidote, ilmenite, apatite, rutile and zircon (Fig. 2a–d). The biotite (Bt) gneisses are comprised of plagioclase (~20 vol%), K-feldspar (~35 vol%), quartz (~40 vol%), biotite (~4 vol%), and accessory minerals of allanite, epidote, apatite and zircon (Fig. 2e, f). The foliation is defined by aligned biotite flakes and quartz-feldspar bands. Thereinto, allanite occurs in two ways: those with epidote rims and zircon inclusions (Fig. 2c–e), and those as inclusions within titanite (Fig. 7f, g, m, o, p). Most titanite grains rim ilmenite, and some have inclusions of biotite, allanite, apatite, plagioclase, quartz or minor rutile. The gneisses have a mineral assemblage of plagioclase + K-feldspar + biotite + quartz + epidote ± amphibole ± titanite.

The studied gneisses underwent partial melting as revealed by the following evidence: (1) feldspar grains with cuspate extensions along quartz-quartz contacts (Fig. 2b), (2) narrow trains of K-feldspar blebs along quartz-plagioclase contacts (Fig. 2a, f), (3) adjacent grains of quartz, feldspar and biotite are corroded (Fig. 2a, b, e, f). These microstructures are interpreted as crystallization products of the former melt (e.g., Sawyer, 2001; Brown, 2002; Timmermann et al., 2002).

3. Analytical methods and results

Analytical method details are given in Supplementary Text 1, including

Cathodoluminescence (CL) images, back scattered electron (BSE) images and analytical data on mineral major elements, bulk-rock major and trace elements, Sr–Nd isotopes, zircon U–Pb dating, trace elements and Hf isotopes, and titanite *in situ* U–Pb dating.

3.1. Mineral major element data

Major element compositions of plagioclase and amphibole in the Bt-amp gneiss (samples 169-1 and 39-1) are given in Supplementary Table 1 and 2, respectively.

Plagioclase grains in both samples are oligoclase, with An contents of 0.28–0.30. Amphibole grains have 10.98–11.68 wt% CaO and 1.19–1.42 wt% Na_2O classified as calcic amphibole (Leake et al., 1997).

3.2. Bulk-rock major and trace element and Sr–Nd isotope data

Bulk-rock major element, trace element and Sr–Nd isotopic compositions on the studied samples are given in Table 2.

The Bt-amp gneiss samples (169-1, 169-2 and 39-1) have 64.2–68.4 wt% SiO_2, 15.0–15.7 wt% Al_2O_3, 3.33–3.80 wt% CaO, 3.40–4.10 wt% Na_2O and 2.40–3.72 wt% K_2O. The Bt gneiss samples (168-1 and 169-4) are characterized by higher SiO_2 (70.3–71.9 wt%) and K_2O (4.33–5.34 wt%), but lower Al_2O_3 (13.9–14.7 wt%), CaO (1.85–2.06 wt%) and Na_2O (3.21–3.38 wt%). Using the Ab-An-Or classification for silicic rocks (Barker, 1979), the Bt-amp gneisses are granodiorite whereas the Bt gneisses are granite (Fig. 3a). These granitoid gneisses are metaluminous (Fig. 3b), with the aluminum saturation indices (A/CNK = molecular Al_2O_3 / (CaO + Na_2O + K_2O)) of 0.95–1.02.

These orthogneisses are enriched in light rare earth elements (REE) and relatively depleted in heavy REEs with highly fractionated REE patterns ($(La/Yb)_N$ = 15.3–143.5) and a weak negative Eu anomaly (Eu/Eu* = 0.62–0.87) (Fig. 4a, Table 2). Furthermore, most samples display characteristic arc-like signature of negative Nb, Ta and Ti anomalies (except for sample 169-2 without Ti anomaly due to low REE contents, Fig. 4b).

For the analyzed four samples, their initial $^{87}Sr/^{86}Sr$ isotopic ratios and $\varepsilon_{Nd}(t)$ values calculated at t = 1520 Ma (see 3.3 below). The Bt-amp gneiss samples (169-1, 169-2 and 39-1) have initial $^{87}Sr/^{86}Sr$ ratios of 0.7008–0.7036 and $\varepsilon_{Nd}(t)$ values of -3.6 to +0.1, with model ages T_{DM2} = 2.35–2.05 Ga. The Bt gneiss sample (168-1) gives $\varepsilon_{Nd}(t)$ = -2.2 and T_{DM2} = 2.24 Ga, with an abnormally low $^{87}Sr/^{86}Sr_{initial}$ = 0.6866. This unusual isotopic ratio has no petrogenetic significance because of the mobility of Rb, which led to the excessive subtraction of $^{87}Rb/^{86}Sr$ ratio.

3.3. Zircon U–Pb age and Hf isotope

LA-ICP-MS zircon U–Pb dating and trace element analysis of five samples and zircon Hf isotope compositions of four samples are given in Supplementary Tables 3 and 4, respectively.

Zircon grains from the five gneisses are colorless, subhedral–euhedral oblong or prismatic with varying size of ~ 100–200 μm. CL images show that zircon grains have a core–rim structure consisting of inherited cores with oscillatory zoning and dark rims with weak or no zoning (Figs. 5 and 6). The analyzed spots on zircon cores from two Bt-amp gneiss samples (169-1 and 169-2) and two Bt gneiss samples (168-1 and 169-4) yield weighted mean $^{207}Pb/^{206}Pb$ ages of 1519±36 Ma (n = 5, MSWD = 0.016), 1520±18 Ma (n = 12, MSWD = 0.85), 1516±15 Ma (n = 20, MSWD = 0.046) and 1506±6 Ma (n = 16, MSWD = 0.45), with upper intercept ages of 1544±47 Ma, 1551±23 Ma, 1544±26 Ma and 1498±6 Ma, respectively (Figs. 5a, c and 6a, c). All analyzed spots on core domains have relatively high Th contents (57.7–927 ppm), Th/U ratios (0.10–1.52) and REE contents (170–1576 ppm) with remarkable negative Eu anomalies (Eu/Eu* = 0.07–0.55) (Figs. 5b, d and 6b, d, Supplementary Tables 3). Analyzed spots on zircon rims from three Bt-amp gneiss samples (169-1, 169-2 and 39-1) and one Bt gneiss sample (168-1) yield weighted mean $^{206}Pb/^{238}U$ ages of 605±27 Ma (n = 15, MSWD = 0.96), 591±3 Ma (n = 14, MSWD = 0.54) and 595±2 Ma (n = 21, MSWD = 0.40), with lower intercept ages of 585±11 Ma, 592±18 Ma, 588±6 Ma and 563±10 Ma, respectively (Figs. 5a, c, e and 6a). Only one zircon rim spot from sample 169-2 is obtained with $^{206}Pb/^{238}U$ age of 590±2 Ma (Figs. 5c). Compared with zircon cores, analyzed spots on rim domains have relatively low Th contents (22.0–82.2 ppm), Th/U ratios (0.03–0.10) and REE contents (50.3–473 ppm), with weak or no negative Eu anomalies (Eu/Eu* = 0.21–1.86) (Figs. 5b, d, f and 6a, Supplementary Tables 3).

Therefore, the zircon LA–ICP–MS U–Pb analyses yield two age groups: 1520–1506 Ma of weighted mean $^{207}Pb/^{206}Pb$ age for zircon cores and 605–590 Ma of weighted mean $^{206}Pb/^{238}U$ age for zircon rims.

Fifty-three Hf isotopic analyses on zircon cores from two Bt-amp gneiss samples (169-1 and 169-2) and two Bt gneiss samples (168-1 and 169-4) give initial $^{176}Hf/^{177}Hf$ isotopic ratios of 0.281697–0.281891 and $\varepsilon_{Hf}(t)$ values ranging from -4.5 to +2.6, with two-stage model ages T_{DM2} of 2.54–2.10 Ga (Supplementary Tables 4).

3.4. Titanite *in situ* U–Pb age

Two titanite-rich gneiss samples (169-1 and 39-1) were selected for LA-ICP-MS titanite *in situ* U–Pb dating. BSE images and photomicrographs of representative titanite are shown in Fig. 7 and the titanite U–Pb dating and trace element data are given in Supplementary Table 5.

Most titanite crystals are brown and subhedral–anhedral in shape with inclusions of ilmenite, biotite, allanite, apatite, plagioclase, quartz and minor rutile (Fig. 7). BSE images show that the titanite crystals mostly have patchy zoning. The analyzed spots of titanite yield lower intercept ages are 25.1±0.6 Ma for sample 169-1 (Fig. 8a) and 24.7±0.5 Ma for sample 39-1 (Fig. 8b). After correction using ^{207}Pb, the weighted mean $^{206}Pb/^{238}U$ ages are 26.2±0.4 Ma (n=40, MSWD=2.5) and 26.0±0.6 Ma (n=29, MSWD=3.1) (Fig. 8).

4. Metamorphic *P–T* conditions

4.1. Hbl-Pl-Q thermobarometry

Amphibole–plagioclase thermometry (Holland and Blundy, 1994) and amphibole–plagioclase–quartz barometry (Bhadra and Bhattacharya, 2007) are used to calculate the metamorphic *P–T* condition of the Bt-amp gneisses. The amphibole–plagioclase–quartz thermobarometry yields metamorphic *P–T* conditions of 6.2–7.2 kbar and 691–736 °C for sample 169-1, and 5.4–6.5 kbar and 716–765 °C for sample 39-1.

4.2. Zr-in-titanite thermometry

Titanite formation temperatures are estimated using the Zr-in-titanite thermometry (T (°C) = $[7708 + 960P] / [10.52 - \log(\alpha_{TiO2}) - \log(\alpha_{SiO2}) - \log(\text{ppm Zr, titanite})] - 273$; Hayden et al., 2008). The activity of TiO_2 is assumed to be 0.5 (plausible lower limits in typical crustal rocks), with SiO_2 activity assumed as 1.0 (Hayden and Watson 2007; Ferry and Watson 2007). Based on amphibole–plagioclase–quartz barometer, the metamorphic pressure conditions of the Bt-amp gneisses are ~ 6 kbar. Zr concentrations range from 158 to 591 ppm in sample 169-1, and from 276 ppm to 620 ppm in sample 39-1. The calculations of Zr-in-titanite thermometry are 688–756 °C for sample 169-1 and 716–759 °C for sample 39-1 (Supplementary Table 5). The temperature data display a cluster at 700–750 °C (64/69, Fig. 9), which is consistent with the temperature conditions obtained by the amphibole–plagioclase thermometry.

5. Discussion

5.1. Age interpretation

Zircon LA-ICP-MS U–Pb dating shows two age groups of 1520–1506 Ma and 605–590 Ma. Most zircons of the studied Dongjiu gneisses show euhedral-prismatic forms and display rounded terminations, which in some cases generate an ovoid morphology. CL images show that all zircon grains have a core–rim structure, i.e., oscillatory-zoned core and rim with weak or no zoning (Figs. 5 and 6). The inherited zircon cores yield concordant ages of 1520–1506 Ma without detrital age distribution (analyses with concordance > 95%, Supplementary Tables 3). These zircon cores have relatively high Th contents (usually > 50 ppm) with high Th/U ratios (⩾ 0.1, up to 1) (Fig. 10) and REE patterns with remarkable negative Eu anomalies (Figs. 5b, d and 6b, d). These properties are consistent with the zircons of magmatic origin (e.g., Hoskin and Schaltegger, 2003). Thus, the Mesoproterozoic age of ~ 1500 Ma given by the zircon cores represents the protolith crystallization age of the gneisses. By comparison, CL images show that zircon rims have weak or no zoning. Most zircon rims occur as lobes with smooth or rough edges, and may overprint pre-existing structures (Fig. 5b, f). All these characteristics suggest that zircon rims have developed during metamorphic recrystallization near the solidus (Hoskin and Black, 2000; Rubatto, 2017). The zircon rims have lower Th contents (usually < 50 ppm) and

Th/U ratios (< 0.1) (Fig. 10) without remarkable negative Eu anomalies (Figs. 5b, d, f and 6b), which are consistent with metamorphic zircon (e.g., Rubatto et al., 2009; Rubatto, 2017). Based on the zircon internal structure, Th/U ratios and REE patterns, we suggest that the zircon rims provide the metamorphic ages of 605–590 Ma for the orthogneisses in the Dongjiu area.

Titanite crystals from two Bt-amp gneiss samples are subhedral–anhedral in shape with metamorphic mineral inclusions of ilmenite, biotite, allanite, plagioclase, quartz or minor rutile (Fig. 7). BSE images show that titanite crystals have patchy zonation, characteristic of metamorphic titanite (Rubatto, 2017). Therefore, LA–ICP–MS titanite *in situ* U–Pb dating indicates that these gneisses experienced Oligocene metamorphism at ~ 26 Ma.

In summary, the protoliths of the gneisses from the Dongjiu area crystallized in the Mesoproterozoic (1520–1506 Ma), and followed by subsequent metamorphism in the Neoproterozoic (605–590 Ma) and more recently in the Oligocene (~ 26 Ma).

5.2. Mesoproterozoic magmatism

The Lhasa terrane, as the southernmost part of the Asian continent, experienced intense deformation, magmatism and metamorphism related to the northward Neo-Tethyan seafloor subduction in the Mesozoic and the India-Asia continental collision in the Cenozoic (e.g., Zhu et al., 2011; Zhang et al., 2014a). Due to these strong reworking processes, the Precambrian thermotectonic records are rarely reported (e.g., Dong et al., 2010, 2011b; Guynn et al., 2012; Zhang et al., 2012b; Xu et al., 2013a;

Hu et al., 2018b; Chen et al., 2019).

Based on the zircon U–Pb geochronology, the inherited magmatic zircon cores of the Dongjiu gneisses yield crystallization ages of 1520–1506 Ma (lack detrital components; see above), indicate that the protoliths of Dongjiu gneisses are Mesoproterozoic magmatic rocks. The bulk-rock chemical compositions of the Dongjiu gneisses suggest that their protoliths are metaluminous granodiorite and granite (Fig. 3), characteristic of arc-like signature with negative Nb, Ta and Ti anomalies (Fig. 4b). The Mesoproterozoic granitic rocks have bulk-rock $\varepsilon_{Nd}(t)$ values of -3.6 to +0.1 and zircon $\varepsilon_{Hf}(t)$ values of -4.5 to +2.6, with similar T_{DM2} ages of 2.35–2.05 Ga and 2.54–2.10 Ga respectively, suggesting that the magmatic rocks are derived from partial melting of Paleoproterozoic crustal material.

The coeval ~ 1500 Ma magmatic rocks are widespread in several continental fragments, including West Africa, South America, North America, Australia, Baltica (Northern Europe), Siberia and India. The rock types are mainly mafic dikes and sills (e.g., Ernst et al., 2013, 2016; Silveira et al., 2013), and massif-type anorthosites (e.g., Emslie, 1978; Weis, 1986; Sadowski and Bettencourt, 1996; Mukherjee and Das, 2002). The Mesoproterozoic Era, dominated by the break-up of the Columbia supercontinent and the formation of the Rodinia supercontinent, was an important crust-forming period in many continents in Earth's history. The global Mesoproterozoic magmatism has commonly been attributed to the rifting and fragmentation of the Columbia supercontinent (e.g., Rogers and Santosh, 2002; Zhao et al., 2003). However, ~ 1.6–1.5 Ga metamorphic and magmatic rocks of the Central

Indian Tectonic Zone are the products of south-north Indian subcontinental collision (e.g., Acharyya, 2003; Kröner et al., 2012). For the studied Mesoproterozoic granitic rocks in the SLT, it is too difficult to discuss the tectonic setting in a global context owing to their limited distribution and subsequent reworking.

The Mesoproterozoic inherited zircons in the Gangdese batholith (e.g., Zhu et al., 2011; Ji et al., 2017), and detrital zircons from the sedimentary rocks of the Carboniferous–Triassic strata (Leier et al., 2007; Pullen et al., 2008; Dong et al., 2010; Zhu et al., 2013; Li et al., 2014; Guo et al., 2017) indicate that the Mesoproterozoic magmatic rocks are probably more widely distributed than exposed in the Lhasa terrane. Moreover, the metasedimentary rocks from the Nyingchi complex in the SLT contain abundant ~1500 Ma detrital zircons (Guo et al., 2017). The 1550–1450 Ma detrital zircons from the CLT Permian–Triassic strata define a broad band of $\varepsilon_{Hf}(t)$ values (-16.7 to +9.6; Fig. 11). By comparison, the coeval detrital zircons from the SLT metasedimentary rocks have lower $\varepsilon_{Hf}(t)$ values (-11.3 to +3.2; Fig. 11). The studied Mesoproterozoic granitic rocks, with the coeval gneisses of the southern Nyingchi complex (our unpublished data) have the similar zircon $\varepsilon_{Hf}(t)$ values as the above, suggesting that they might be local sources for the Mesoproterozoic detrital zircons of the Paleozoic strata (Fig. 11).

5.3. Neoproterozoic and Oligocene metamorphism

Based on zircon and titanite U–Pb geochronology, the Dongjiu orthogneisses experienced two metamorphic events at 605–590 Ma recorded by zircon and 26 Ma by titanite, respectively.

5.3.1. Neoproterozoic metamorphism

Due to the Oligocene metamorphism, the Neoproterozoic metamorphic minerals are usually overprinted. The petrography shows that ilmenite is all surrounded by titanite; rare rutile only occurs as inclusions within titanite; and allanite is rimed by epidote including zircon grains (Figs. 2c, d and 7). Along with titanite formed in the later metamorphism, we speculate that the mineral assemblage of the Neoproterozoic metamorphism is represented as ilmenite and allanite. Lacking index metamorphic minerals, it is difficult to calculate the detailed *P*–*T* conditions of the Neoproterozoic metamorphism for the studied gneisses. However, the characteristics of zircon internal structure and chemistry show that zircon rims of the Dongjiu gneisses likely form under conditions near solidus. Rubatto et al. (2009) show that the metamorphic zircon rims of metatonalite with the similar mineral assemblage to this study formed under amphibolite-facies condition (T = 620–700 ºC). For diorite bulk composition, recent phase equilibrium modeling indicated that the H_2O-saturated (wet) solidus occurs between ~ 650–700 °C and garnet becomes stable above ~ 8.5 kbar (e.g., Palin et al., 2016). On the formation condition of zircon rim, bulk composition and lack of garnet, we reason that the Dongjiu granitic gneisses underwent MP amphibolite-facies metamorphism at 605–590 Ma.

According to the Gondwana-derived affinity, the ~ 600 Ma metamorphic event of the Lhasa terrane is likely related to the assembly of Gondwana supercontinent (e.g., Meert, 2003; Veevers, 2004; Collins and Pisarevsky, 2005). Early palaeogeographic models based on limited data interpreted the presence of a single super-continent throughout the Proterozoic (Piper, 1976). McWilliams (1981) suggested that two Neoproterozoic continental masses, East Gondwana (India, East Australia, Antarctica, Madagascar and Sri Lanka) and West Gondwana (Africa and South America) collided along the Mozambique Belt to form Gondwana. Form the Rodinia fragments to the final amalgamation Gondwana, there have been many accretionary terranes and collisional events (Collins and Pisarevsky, 2005). Although more work is needed on details of such amalgamation. Meert and co-workers (Meert, et al., 1995; Meert and Van der Voo, 1997; Meert, 2001, 2003) suggested a multiphase assembly of two main periods of orogenesis, including an earlier East African Orogeny (EAO) (~ 750–620 Ma) and a later Kuunga Orogeny (~ 570–530 Ma). The later orogeny marks the collision of Australia and Antarctica with the rest of Gondwana and was subsequently correlated with a broad belt of orogenesis from the Damara Orogen in the west to the Pinjarra Orogen in the east (Meert, 2003). They proposed a Neoproterozoic continent consisting of Sri Lanka, Madagascar and India colliding with a combined Congo/Kalahari (African) continent at ~ 750–620 Ma, followed by Australia/East Antarctica colliding with the bulk of Gondwana at ~ 570–530 Ma (Meert, 2003; Meert and Torsvik, 2003). However, Boger and Miller (2004) proposed that the EAO evolved as an accretionary orogeny and was partially superimposed by a ~ 590–560 Ma orogen created by the collision of combined India, Madagascar and part of Antarctica land masses with eastern Africa along the

Mozambique suture. In their model, Australia–Antarctica collided with India along the Kuunga suture at ~ 535–520 Ma. Until now, the Precambrian metamorphic events of the Lhasa terrane are only reported in the Nyainqêntanglha Group in the central CLT (~ 690–650 Ma, Dong et al., 2011b; Zhang et al., 2012b), the Bomi complex in the eastern CLT (~ 625–600 Ma, Chen et al., 2019), and the Nyingchi complex in the eastern SLT (~ 600 Ma, Lin et al., 2013b and this study). The Nyainqêntanglha Group experienced an early granulite-facies peak-metamorphism at ~ 690–650 Ma, and late amphibolite-facies retrogression at ~ 480 Ma (Dong et al., 2011b; Zhang et al., 2012b). Zhang et al. (2012b, 2014a) suggested that the Neoproterozoic metamorphism occurred during the assembly of East and West Gondwana within the EAO. For all other Precambrian metamorphic events, only the Nyingchi complex is speculated to experience MP amphibolite-facies metamorphism without knowing exact *P*–*T* conditions due to the Cenozoic metamorphic reworking. Therefore, this study suggests that the ~ 600 Ma metamorphism events recorded in the Nyingchi complex in the eastern SLT and the Bomi complex in the eastern CLT are likely response to the assembly of Gondwana supercontinent.

5.3.2. Oligocene metamorphism and melting

In this study, titanite formed at ca. 26 Ma is observed either mostly riming ilmenite or as separate grains. Titanite can be in contact with a variety of minerals, e.g., amphibole, biotite, plagioclase and epidote, and contains inclusions of biotite, allanite, plagioclase and quartz (Fig. 7). The formation of titanite rims on the ilmenite could be explained in terms of reactions such as: ilmenite + allanite + K-feldspar + quartz = titanite + anorthite + annite + H_2O (Harlov et al., 2006; Angiboust and Harlov, 2017). Titanite rimming ilmenite is commonly present in the amphibolite-facies rocks (e.g., Nijland and Maijer, 1993; Nijland and Visser, 1995; Hansen et al., 2002; Harlov and Hansen, 2005). The mineral assemblage (plagioclase + K-feldspar + biotite + quartz + epidote ± amphibole ± titanite) also indicates that the later Oligocene metamorphism occurred at amphibolite-facies condition. Hbl-Pl-Q thermobarometry shows that the Dongjiu gneisses experienced peak P–T conditions of 5.4–7.2 kbar and 691–765 °C. Zr-in-titanite thermometry yields the similar T conditions of 688–759 °C at ~ 6 kbar. Moreover, the microstructure proves that these studied gneisses record the presence of melt. Therefore, we suggest that the prior melt represents the product of the Oligocene metamorphism, and the Dongjiu gneisses underwent MP amphibolite-facies metamorphism and melting at ca. 26 Ma. In the southern part of the studied area, the coeval metamorphic rocks of the Nyingchi complex have also been reported to take place under amphibolite-facies conditions (e.g., Zhang et al., 2010; Dong et al., 2012; Palin et al., 2014; Kang et al., 2019).

5.4. The nature of the Precambrian basement of the Lhasa terrane

The spatial distribution and nature of the Precambrian basement beneath the entire Lhasa terrane have been speculative. Duo to medium- to high-grade metamorphism, the Nyainqêntanglha Group in the CLT and the Nyingchi complex in the SLT have been regarded as the Precambrian metamorphic basement (Xu et al.

1985; Dewey et al. 1988; Harris 1988b; Hu et al. 2005). However, adequate age constraints are lacking. Based on zircon Hf isotope data, Zhu et al (2011) suggested that the CLT has ancient basement rocks of Proterozoic and Archean ages with NLT and SLT being younger and juvenile crust (Phanerozoic) accreted towards the CLT.

The Amdo basement, consisting of orthogneisses and mafic granulites, is reported to represent the Precambrian basement of the Lhasa terrane (Xu et al., 1985; Coward et al., 1988; Kidd et al., 1988; Pan et al., 2004). The gneisses have crystallization ages of Neoproterozoic (~820 Ma; Zhang et al., 2012a) and Cambro-Ordovician (540–460 Ma; Xu et al., 1985; Xie et al., 2010; Guynn et al., 2012; Zhang et al., 2012a). The mafic granulites have undergone peak granulite-facies metamorphism at ~ 190 Ma and retrogressed under amphibolite-facies conditions at ~ 180 Ma (e.g., Xu et al., 1985; Guynn et al., 2006; Zhang et al., 2012a; Zhang XR et al., 2014). Therefore, the Amdo gneiss represents a Neoproterozoic crystallization basement, which undergoes metamorphism in the early Jurassic.

The existence of a Precambrian basement in the CLT has been previously inferred using older inherited zircon ages of the gneiss (Allégre et al., 1984) and the bulk-rock Nd isotope composition from sedimentary rocks (Zhang KJ et al., 2007). Recently reported old rocks are the ca. 925–748 Ma granitoids and gabbros of the Nyainqêntanglha Group in the Xianza area west of Nam Tso Lake (Hu et al., 2005; Zhang et al., 2012b; Hu et al., 2018 a, b; Zeng et al., 2018). These rocks have experienced granulite-facies peak-metamorphism at ca. 690–650 Ma (Dong et al., 2011b; Zhang et al., 2012b). Some studies suggest that the Neoproterozoic magmatic rocks are crust of the Mozambique Ocean (Zhang et al., 2012b; Zeng et al., 2018), but others propose that these rocks formed in a back-arc setting (Hu et al., 2018 a, b). In addition, the Bomi complex consists of the Proterozoic magmatic rocks formed at ca. 1866 Ma, 1343–1250 Ma and 824 Ma, and undergoes metamorphism at ca. 625–600 Ma and 80 Ma (Xu et al., 2013a; Chen et al., 2019). Thereinto, the Paleoproterozoic and Neoproterozoic granitoid gneisses show geochemical affinity of volcanic arc granites (Chen et al., 2019); the Mesoproterozoic granite gneisses have an aluminous A-type granite affinity (Xu et al., 2013a). However, there is no constraint on the metamorphic condition. Therefore, the CLT indeed has Proterozoic basement.

In the SLT, the Nyingchi complex has been interpreted to represent slivers of a Precambrian basement of the Lhasa terrane (e.g., Pan et al., 2004; Xie et al., 2007; Yin et al., 2003). However, more recent studies suggested that most high-grade metamorphic rocks in the eastern SLT underwent Mesozoic to Cenozoic metamorphism and their protoliths included both sedimentary and magmatic rocks with various protolith ages (Dong et al., 2010, 2012, 2014; Guo et al., 2011, 2012, 2017; Palin et al., 2014; Xu et al., 2013b; Zhang et al., 2010, 2013, 2014a, 2014b, 2015). Here, the Dongjiu gneisses, as a part of the Nyingchi complex, have a protolith crystalline age of 1520–1506 Ma, and experienced amphibolite-facies metamorphism at 605–590 Ma, representing a Precambrian metamorphic basement of the SLT. Moreover, the studied Mesoproterozoic granitic rocks have T_{DM2} of 2.54–2.10 Ga, along with Meso- to Paleoproterozoic zircon Hf model ages of Cambrian and Devonian–Carboniferous granitoids (Ji et al., 2012; Dong et al., 2014, 2015), implying the presence of an older early Paleoproterozoic curst yet unidentified in the SLT.

Excluding the ca. 1780 Ma xenoliths reported by Lin et al. (2013b), the ~ 1500 Ma granitic gneisses from the Dongjiu area here are the oldest rocks reported of the SLT. The zircon Hf and bulk-rock Nd isotopes give similar T_{DM2} ages up to 2.5 Ga, suggesting that the Mesoproterozoic granitic rocks are derived from melting of the Paleoproterozoic crustal material. Moreover, the ~ 1500 Ma gneisses from the southern Nyingchi complex give Paleoproterozoic zircon Hf model ages (Fig. 11, our unpublished data). By comparison, the Proterozoic granitoids from the Bomi complex in the CLT have similar zircon Hf T_{DM2} ages ranging from 2.5 to 1.3 Ga (Xu et al., 2013a; Chen et al., 2019). Furthermore, the magmatic rocks (before 360 Ma) from both the SLT and CLT have the same ranges of zircon $\varepsilon_{Hf}(t)$ values and model ages (Fig. 11). Therefore, we suggest that the SLT and CLT share a common Precambrian basement.

5.5. Reworking of the Precambrian basement of the Lhasa terrane

Although both SLT and CLT share a common Precambrian basement, the strong thermal events (including metamorphism and mainly mantle-derived magmatism) as a consequence of the northward subduction of the Neo-Tethyan seafloor beneath the Lhasa terrane and the subsequent India-Asia continental collision have intensively reworked the Precambrian basement.

Since the early Mesozoic, important mantle contributions have caused the drastically elevated zircon $\varepsilon_{Hf}(t)$ of the magmatic rocks from the SLT (Fig 11). However, their zircon $\varepsilon_{Hf}(t)$ values vary significantly (up to 20 units from ~ -5 to +15; Fig. 11), indicating the presence of old basement. The input of mantle material not only contributed to juvenile continental crust growth (e.g., Mo et al., 2007; Zhu et al., 2011), but also reworked the Precambrian basement of the SLT. In contrast, the granitoids from the CLT exhibit negative zircon $\varepsilon_{Hf}(t)$ and old T_{DM2} ages, suggesting that they are mainly derived from partial melting of ancient continental crust. Therefore, the basement of the CLT underwent weaker reworking, preserving more rocks with Nd-Hf isotopes characteristic of ancient continental crust than the SLT.

This study shows that the Precambrian metamorphic basement of the Lhasa terrane has also undergone more recent metamorphism at ~ 26 Ma. Due to similar metamorphic conditions, it is difficult to distinguish mineral assemblages as the result of recent metamorphism from those of the Neoproterozoic metamorphism, except for the preserved inclusions of ilmenite and allanite. The main mineral assemblage of plagioclase + K-feldspar + biotite + quartz + epidote ± amphibole ± titanite is the product of the Oligocene metamorphism. The coeval metamorphic rocks have been widely reported in the south part of the Nyingchi complex (e.g., Zhang et al., 2010, 2014a; Guo et al., 2011; Dong et al., 2012; Palin et al., 2014; Kang et al., 2019). Zhang et al. (2015) suggested that the crustal shortening and thickening resulting from the continental collision and continued convergence is the very tectonic mechanism for the Oligocene reworking of the Lhasa terrane crust.

6. Conclusion

(1) The protoliths of the Dongjiu orthogneisses in the SLT are granodiorite and granite emplaced at 1520–1506 Ma, which provide source materials for the Paleozoic metasedimentary rocks in the Lhasa terrane. The Mesoproterozoic granitoids have derived from partial melting of earlier Paleoproterozoic crustal material.

(2) The Mesoproterozoic orthogneisses from the Dongjiu area have experienced the Neoproterozoic (605–590 Ma) metamorphism, and therefore represent the Precambrian metamorphic basement of the SLT.

(3) The Dongjiu gneisses also underwent the Oligocene (26 Ma) metamorphism under MP amphibolite-facies conditions as the result of crustal shortening and thickening in response to the continued India-Asia continental convergence.

(4) The CLT and SLT share a common Precambrian metamorphic basement, but the SLT basement has been strongly reworked by mantle-derived magmatism and metamorphism since the Mesozoic.

Acknowledgments

We want to thank two anonymous journal referees and Editor Guochun Zhao for their constructive comments, which have helped improve the quality of this paper. This study was supported by the National Natural Science Foundation of China (grants 41872070 and 91855210) and the China Geological Survey (grants

DD20160122 and DD20190057). Xin Dong acknowledges the China Scholarship Council for funding a 12-month research at Durham University, UK (CSC NO. 201809110024). We thank Dr. Zhenyu He, Hua Xiang and Fenghua Liang for their support of this work; Dr. Zhengbin Gou and Huixia Ding for taking part in field work, and Ph.D. students Yanhong Chen and Fangyu Shen for helpful discussion.

References

Acharyya, S.K., 2003. The Nature of Mesoproterozoic Central Indian Tectonic Zone with Exhumed and Reworked Older Granulites. Gondwana Res. 6 (2), 197–214.

Allégre, C.J., et al., 1984. Structure and evolution of the Himalaya–Tibet orogenic belt. Nature 307, 17–22.

Angiboust, S., Harlov, D., 2017. Ilmenite breakdown and rutile-titanite stability in metagranitoids: Natural observations and experimental results. Am. Mineral. 102 (8), 1696–1708.

Barker, F., 1979. Trondhjemite: definition environment and hypothesis of origin. In: Barker F (Ed) Trondhjemites dacites and related rocks. Elsevier, Amsterdam, pp. 1–12.

Bhadra, S., Bhattacharya, A., 2007. The barometer tremolite + tschermakite + 2 albite = 2 pargasite + 8 quartz: constraints fromexperimental data at unit silica activity, with application to garnet-free natural assemblages. Am. Mineral. 92 (4), 491–502.

Boger, S.D., Miller, J.M., 2004. Terminal suturing of Gondwana and the onset of the Ross–Delamerian Orogeny: The cause and effect of an Early Cambrian reconfiguration of plate motions. Earth Planet. Sci. Lett. 219, 35–48.

Booth, A.L., Zeitler, P.K., Kidd, W.S.F., Wooden, J., Liu, Y.P., Idleman, B., Hren, M., Chamberlain, C.P., 2004. U–Pb zircon constraints on the tectonic evolution of southeastern Tibet, Namche Barwa area. Am. J. Sci. 304 (10), 889–929.

Brown, M., 2002. Retrograde processes in migmatites and granulites revisited. J. Metamorph. Geol. 20 (1), 25–40.

Chang, C.F., et al., 1986. Preliminary conclusions of the Royal Society and Academia-Sinica 1985 Geotraverse of Tibet. Nature 323, 501–507.

Chang, C.F., Zheng, S.L., 1973. Tectonic features of the Mount Jolmo Lungma region in southern Tibet, China. Chin. J. Geol. 1 (1), 1–12.

Chen, L.R, Xu, W.C., Zhang, H.F., Zhao, P.L., Guo, J.L., Luo, B.J., Guo, L., Pan, F.B., 2019. Origin and early evolution of the Lhasa Terrane, South Tibet: Constraints from the Bomi Gneiss Complex. Precambrian Res. 331, 105360.

Chen, Z.J., Tian, Z.L., Zhang, Z.M., Dong, X., 2017. Early Jurassic metamorphism of the eastern segment of the Lhasa terrane in south Tibet and its tectonic significance. Int. Geol. Rev. 59 (14), 1–17.

Cheng, H., Liu, Y., Vervoort, J.D., Lu, H., 2015. Combined U–Pb, Lu–Hf, Sm–Nd and Ar–Ar multichronometric dating on the Bailang eclogite constrains the closure timing of the Paleo-Tethys Ocean in the Lhasa terrane, Tibet. Gondwana Res. 28 (4), 1482–1499.

Chiu, H.Y., Chung, S.L., Wu, F.Y., Liu, D.Y., Liang, Y.H., Lin, Y.J., Iizuka, Y., Xie, L.W., Wang, Y.B., Chu, M.F., 2009. Zircon U–Pb and Hf isotope constraints from eastern Transhimalayan batholiths on the precollisional magmatic and tectonic evolution in southern Tibet. Tectonophysics 477 (1–2), 3–19.

Chu, M.F., Chung, S.L., Song, B., Liu, D.Y., O'Reilly, S.Y., Pearson, N.J., 2006. Zircon U–Pb and Hf isotope constraints on the Mesozoic tectonics and crustal evolution of southern Tibet. Geology 34 (9), 745–748.

Collins, A.S., Pisarevsky, S.A., 2005. Amalgamating eastern Gondwana: The evolution of the circum-Indian orogens. Earth Sci. Rev. 71, 229–270.

Coward, M.P., Kidd, W.F., Yun, P., Shackleton, R.M., Zhang, H., 1988. The structure of the 1985 Tibet Geotraverse, Lhasa to Golmud. Phil. Trans. Roy. Soc. Lond. A 327, 307–336.

Dewey, J.F., Shackelton, R.M., Chang, C., Sun, Y., 1988. The tectonic evolution of the Tibetan Plateau. Phil. Trans. Roy. Soc. Lond. A 327, 379–413.

Ding, H.X., Zhang, Z.M., Dong, X., Yan, R., Lin, Y.H., Jiang, H.Y., 2015. Cambrian ultrapotassic rhyolites from the Lhasa terrane, south Tibet: Evidence for Andean-type magmatism along the northern active margin of Gondwana. Gondwana Res. 27 (4), 1616–1629.

Ding, L., Kapp, P., Zhong, D., Deng, W., 2003. Cenozoic volcanism in Tibet: Evidence for a transition from oceanic to continental subduction. J. Petrol. 44, 1833–1865.

Dong, X., Zhang, Z.M., Santosh, M., 2010. Zircon U–Pb chronology of the Nyingtri

Group, Southern Lhasa Terrane, Tibetan Plateau: Implications for Grenvillian and Pan-African provenance and Mesozoic-Cenozoic metamorphism. J. Geol. 118 (6), 677–690.

Dong, X., Zhang, Z.M., Liu, F., Wang, W., Yu, F., Shen, K., 2011a. Zircon U–Pb geochronology of the Nyainqêntanglha Group fromthe Lhasa terrane: New constraints on the Triassic orogeny of the south Tibet. J. Asian Earth Sci. 42 (4), 732–739.

Dong, X., Zhang, Z.M., Santosh, M., Wang, W., Yu, F., Liu, F., 2011b. Late Neoproterozoic thermal events in the northern Lhasa terrane, south Tibet: Zircon chronology and tectonic implications. J. Geodyn. 52 (5), 389–405.

Dong, X., Zhang, Z.M., Liu, F., Wang, W., Yu, F., Lin, Y.H., Jiang, H.Y., He, Z.Y., 2012. Genesis of the metamorphic rocks from southeastern Lhasa terrane and the Mesozoic-Cenozoic orogenesis. Acta Petrol. Sin. 28 (6), 1765–1784 (in Chinese with English abstract).

Dong, X., Zhang, Z.M., 2013. Genesis and tectonic significance of the Early Jurassic magmatic rocks from the southern Lhasa terrane. Acta Petrol. Sin. 29 (6), 1933–1948 (in Chinese with English abstract).

Dong, X., Zhang, Z.M., Liu, F., He, Z.Y., Lin, Y.H., 2014. Late Paleozoic intrusive rocks from the southeastern Lhasa terrane, Tibetan Plateau, and their Late Mesozoic metamorphism and tectonic implications. Lithos 198–199, 249–262.

Dong, X., Zhang, Z.M., 2015. Cambrian granitoids from the southeastern Tibetan Plateau: Research on petrology and zircon Hf isotope. Acta Petrol. Sin. 31 (5), 1183–1199 (in Chinese with English abstract).

Emslie, R.F., 1978. Anorthosite massifs, rapakivi granites, and late Proterozoic rifting of North America. Precambrian Res. 7 (1), 61–98.

Ernst, R.E., Pereira, E., Hamilton, M.A., Pisarevsky, S.A., Rodriques, J., Tassinari, C.C.G., Teixeira, W., Van-Dunem, V., 2013. Mesoproterozoic intraplate magmatic 'barcode' record of the Angola portion of the Congo Craton: Newly dated magmatic events at 1505 and 1110 Ma and implications for Nuna (Columbia) supercontinent reconstructions. Precambrian Res. 230, 103–118.

Ernst, R.E., Okrugin, A.V., Veselovskiy, R.V., Kamo, S.L., Hamilton, M.A., Pavlov, V., Söderlund, U., Chamberlain, K.R., Rogers, C., 2016. The 1501 Ma kuonamka large igneous province of northern siberia: U–Pb geochronology, geochemistry, and links with coeval magmatism on other crustal blocks. Russ. Geol. Geophys. 57 (5), 653–671.

Ferry, J.M., Watson, E.B., 2007. New thermodynamic models and revised calibrations for the Ti-in-zircon and Zr-in-rutile thermometers. Contrib. Mineral. Petrol. 154 (4), 429–437.

Guo, L., Zhang, H.F., Harris, N., Pan, F.B., Xu, W.C., 2011. Origin and evolution of multistage felsic melts in eastern Gangdese belt: Constraints from U–Pb zircon dating and Hf isotopic composition. Lithos 127 (1–2), 54–67.

Guo, L., Zhang, H.F., Harris, N., Parrish, R., Xu, W.C., Shi, Z.L., 2012. Paleogene crustal anatexis and metamorphism in Lhasa terrane, eastern Himalayan syntaxis: Evidence from U–Pb zircon ages and Hf isotopic compositions of the Nyingchi

Complex. Gondwana Res. 21 (1), 100–111.

Guo, L., Zhang, H.F., Harris, N., Xu, W.C., Pan, F.B., 2017. Detrital zircon U–Pb geochronology, trace-element and Hf isotope geochemistry of the metasedimentary rocks in the eastern Himalayan syntaxis: Tectonic and paleogeographic implications. Gondwana Res. 41, 207–221.

Guo, L.S., Liu, Y.L., Liu, S.W., Cawood, P.A., Wang, Z.H., Liu, H.F., 2013. Petrogenesis of Early to Middle Jurassic granitoid rocks from the Gangdese belt, Southern Tibet: Implications for early history of the Neo-Tethys. Lithos 179, 320–333.

Guynn, J.H., Kapp, P., Pullen, A., Heizler, M., Gehrels, G., Ding, L., 2006. Tibetan basement rocks near Amdo reveal "missing" mesozoic tectonism along the Bangong suture, central Tibet. Geology 34 (6), 505–508.

Guynn, J., Kapp, P., George, E., Ding, L., 2012. U–Pb geochronology of terrane rocks in central Tibet and paleogeographic implications. J. Asian Earth Sci. 43 (1), 23–50.

Hansen, E.C., Ahmed, K., Harlov, D.E., 2002. Rb depletion in biotites and whole rocks across an amphibolite to granulite-facies transition zone, Tamil Nadu, South India. Lithos 64 (1), 29–47.

Harlov, D.E., Hansen, E.C., 2005. Oxide and sulphide isograds along a late Archean, deep-crustal profile in Tamil Nadu, South India. J. Metamorph. Geol. 23 (4), 241–259.

Harlov, D.E., Tropper, P., Seifert, W., Nijland, T., Förster, H.J., 2006. Formation of

Al-rich titanite ($CaTiSiO_4O$–$CaAlSiO_4OH$) reaction rims on ilmenite in metamorphic rocks as a function of $f$$H_2O$ and $f$$O_2$. Lithos 88, 72–84.

Harris, N.B.W., Xu, R.H., Lewis, C.L., Hawkesworth, C.L., Zhang, Y.Q., 1988a. Isotope geochemistry of the 1985 Tibet Geotraverse, Lhasa to Golmud. Phil. Trans. Roy. Soc. Lond. A 327, 263–285.

Harris, N.B.W., Holland, T.J.B., Tindle, A.G., 1988b. Metamorphic rocks of the 1985 Tibet Geotraverse, Lhasa to Golmud. Phil. Trans. Roy. Soc. Lond. A 327, 203–213.

Hayden, L.A., Watson, E.B., 2007. Rutile saturation in hydrous siliceous melts and its bearing on Ti-thermometry of quartz and zircon. Earth Planet. Sci. Lett. 258 (3–4), 561–568.

Hayden, L.A., Watson, E.B., Wark, D.A., 2008. A thermobarometer for sphene (titanite). Contrib. Mineral. Petrol. 155 (4), 529–540.

Holland, T.J.B., Blundy, J.D., 1994. Non-ideal interactions in calcic amphiboles and their bearing on amphibole–plagioclase thermometry. Contrib. Mineral. Petrol. 116 (4), 433–447.

Hoskin, P.W.O., Black, L.P., 2000. Metamorphic zircon formation by solid-state recrystallization of protolith igneous zircon. J. Metamorph. Geol. 18 (4), 423–439.

Hoskin, P.W.O., Schaltegger, U., 2003. The composition of zircon and igneous and metamorphic petrogenesis. Rev. Mineral. Geochem. 53 (1), 27–62.

Hou, Z.Q, Duan, L.F, Lu, Y.J, Zheng, Y.C, Zhu, D.C., Yang, Z.M., Yang, Z.S., Wang, B.D., Pei, Y.R., Zhao, Z.D., Mccuaig, T.C., 2015. Lithospheric architecture of the Lhasa terrane and its control on ore deposits in the Himalayan-Tibetan orogen. Econ. Geol. 110, 1541–1575.

Hu, D.G., Wu, Z.H., Jiang, W., Shi, Y.R., Ye, P.S., Liu, Q.S., 2005. SHRIMP zircon U–Pb age and Nd isotopic study on the Nyainqêntanglha Group in Tibet. Sci. China 48 (9), 1377–1386.

Hu, P.Y, Li, C., Wang, M., Xie, C.M, Wu, Y.W., 2013. Cambrian volcanism in the Lhasa terrane, southern Tibet: Record of an early Paleozoic Andean-type magmatic arc along the Gondwana proto-Tethyan margin. J. Asian Earth Sci. 77, 91–107.

Hu, P.Y., Zhai, Q.G., Wang, J., Tang, Y., Wang, H.T., Zhu, Z.C., W, H., 2018a. Middle Neoproterozoic (~ 760 Ma) arc and back-arc system in the North Lhasa terrane, Tibet, inferred from coeval N-MORB- and arc-type gabbros. Precambrian Res. 316, 275–290.

Hu, P.Y., Zhai, Q.G., Wang, J., Tang, Y., Wang, H.T., Hou, K.J., 2018b. Precambrian origin of the north Lhasa terrane, Tibetan Plateau: Constraint from early Cryogenian back-arc magmatism. Precambrian Res. 313, 51–67.

Ji, W.Q., Wu, F.Y., Chung, S.L., Li, J.X., Liu, C.Z., 2009. Zircon U–Pb geochronology and Hf isotopic constraints on petrogenesis of the Gangdese batholith, southern Tibet. Chem. Geol. 262, 229–245.

Ji, W.Q., Wu, F.Y., Chung, S.L., Liu, C.Z., 2012. Identification of early Carboniferous granitoids from southern Tibet and implications for terrane assembly related to the Paleo-Tethyan evolution. J. Geol. 120 (5), 531–541.

Ji, W.Q., Wu, F.Y., Liu, C.Z., Zhang, H., 2017. Zircon U–Pb geochronology and Hf isotopes of granitic rocks and river sands in the Nyingchi region, Tibet: Constraints on evolution of the deep crust beneath the southeast Lhasa terrane. J. Asian Earth Sci. 145, 613–625.

Kang, D.Y., Zhang, Z.M., Dong, X., Tian, Z.L., Xiang, H., Mo, X.X., 2019. Anticlockwise *P-T-t* path and tectonic mechanism of metapelites from the eastern Gangdese arc, southern Tibet. Acta Petrol. Sin. 35 (2), 349–362 (in Chinese with English abstract).

Keto, L.S., Jacobsen, S.B., 1987. Nd and Sr isotopic variations of Early Paleozoic ocean. Earth Planet. Sci. Lett. 84 (1), 27–41.

Kidd, W.F., Pan, Y.S., Chang, C.F., Coward, M.P., Dewey, J.F., Gansser, A., Molnar, P., Shackleton, R.M., Sun, Y.J., 1988. Geological mapping of the 1985 Chinese–British Tibetan (Xizang–Qinghai) Plateau geotraverse route. Phil. Trans. Roy. Soc. Lond. A 327, 287–305.

Kröner, A., Santosh, M., Wong, J., 2012. Zircon ages and Hf isotopic systematics reveal vestiges of Mesoproterozoic to Archaean crust within the late Neoproterozoic-Cambrian high-grade terrain of southernmost India. Gondwana Res. 21 (4), 876–886.

Leake, B.E., et al., 1997. Nomenclature of amphiboles: Report of the subcommittee on amphiboles of the International Mineralogical Association. Commission on New Minerals and Mineral Names. Mineral. Mag. 35, 219–246.

Leier, A.L., Kapp, P., Gehrels, G.E., DeCelles, P.G., 2007. Detrital zircon geochronology of Carboniferous-Cretaceous strata in the Lhasa terrane, southern Tibet. Basin Res. 19 (3), 361–378.

Li, G.W., Sandiford, M., Liu, X.H., Xu, Z.Q., Wei, L.J., Li, H.Q., 2014. Provenance of Late Triassic sediments in central Lhasa terrane, Tibet and its implication. Gondwana Res. 25 (4), 1680–1689.

Li, P., 1955. Primary understanding of geology, eastern Tibet. Chin. Sci. Bull. 7 (7), 62–71 (in Chinese).

Lin, Y.H., Zhang, Z.M., Dong, X., Xiang, H., Yan, R., 2013a, Early Mesozoic metamorphism and tectonic significance of the eastern segment of the Lhasa terrane, south Tibet. J. Asian Earth Sci. 78, 160–183.

Lin, Y.H., Zhang, Z.M., Dong, X., Shen, K., Lu, X., 2013b. Precambrian evolution of the Lhasa terrane, Tibet: Constraint from the zircon U–Pb geochronology of the gneisses. Precambrian Res. 237, 64–77.

Maniar, P.D., Piccoli, P.M., 1989. Tectonic discrimination of granitoids. Geol. Soc. Am. Bull. 101 (5), 635–643.

McWilliams, M.O., 1981. Palaeomagnetism and Precambrian tectonic evolution of Gondwana. In: Kro¨ner, A. (Ed.), Precambrian Plate Tectonics. Elsevier, Amsterdam, pp. 649–687.

Meert, J.G., Van der Voo, R., Ayub, S., 1995. Paleomagnetic investigation of the Neoproterozoic Gagwe lavas and Mbozi complex, Tanzania and the assembly of Gondwana. Precambrian Res. 74 (4), 225–244.

Meert, J.G., Van der Voo, R., 1997. The assembly of Gondwana 800–550 Ma. J. Geodyn. 23 (3–4), 223–235.

Meert, J.G., 2001. Growing Gondwana and rethinking Rodinia: A paleomagnetic perspective. Gondwana Res. 4 (3), 279–288.

Meert, J.G., 2003. A synopsis of events related to the assembly of eastern Gondwana. Tectonphysics 362, 1–40.

Meert, J.G., Torsvik, T.H., 2003. The making and unmaking of a supercontinent: Rodinia revisted. Tectonophysics 375, 261–288.

Meng, Y.K., Dong, H.W., Cong, Y., Xu, Z.Q., Cao, H., 2016. The early-stage evolution of the Neo-Tethys ocean: Evidence from granitoids in the middle Gangdese batholith, southern Tibet. J. Geodyn. 94–95, 34–49.

Mo, X.X., Hou, Z.Q., Niu, Y.L., Dong, G.C., Qu, X.M., Zhao, Z.D., Yang, Z.M., 2007. Mantle contributions to crustal thickening during continental collision: Evidence from Cenozoic igneous rocks in southern Tibet. Lithos 96 (1–2), 225–242.

Mukherjee, A., Das, S., 2002. Anorthosites, Granulites and the Supercontinent Cycle. Gondwana Res. 5 (1), 147–156.

Nijland, T.G., Maijer, C., 1993. The regional amphibolite to granulite facies transition at Arendal, Norway: Evidence for a thermal dome. N. Jahrb. Mineral. Abh. 165, 191–221.

Nijland, T.G., Visser, D., 1995. Provenance of the Bamble amphibolites, Norway. Proc. R. Neth. Acad. Arts Sci. 98 (1–2), 69–88.

Nimaciren, Xie, Y.W., Sha, Z.L., Xiluolangjie, Qiangbazaxi, Peng, D.P., Gesangsuolang, Luosongzhandui, 2005. 1: 250, 000 geological report of Nagqu County with geological map. Xizang Institute of Geological Survey, Lhasa, 103–107 (in Chinese).

Palin, R.M., Searle, M.P., St-Onge, M.R., Waters, D.J., Roberts, N.M.W., Horstwood, M.S.A., Parrish, R.R., Weller, O.M., Chen, S., Yang, J., 2014. Monazite geochronology and petrology of kyanite- and sillimanite-grade migmatites from the northwestern flank of the eastern Himalayan syntaxis. Gondwana Res. 26 (1), 323–347.

Palin, R.M., White, R.W., Green, E.C.R., Diener, J.F.A., Powell, R., Holland, T.J.B., 2016. High-grade metamorphism and partial melting of basic and intermediate rocks. J. Metamorph. Geol. 34, 871–892.

Pan, G.T., Ding, J., Yao, D.S., Wang, L.Q., 2004. Guidebook of 1:1,500,000 geologic map of the Qinghai–Xizang (Tibet) plateau and adjacent areas. Cartographic Publishing House, Chengdu, China, pp. 1–148 (in Chinese).

Pan, G.T., Mo, X.X., Hou, Z.Q., Zhu, D.C., Wang, L.Q., Li, G.M., Zhao, Z.D., Geng, Q.R., Liao, Z.L., 2006. Spatial-temporal framework of the Gangdese Orogenic Belt and its evolution. Acta Petrol. Sin. 22 (3), 521–533 (in Chinese with English abstract).

Piper, J.D.A., 1976. Palaeomagnetic evidence for a Proterozoic super-continent. Phil. Trans. Roy. Soc. Lond. A 280, 469–490.

Pullen, A., Kapp, P., Gehrels, G.E., DeCelles, P.G., Brown, E.H., Fabijanic, J.M., Ding, L., 2008. Gangdese retroarc thrust belt and foreland basin deposits in the Damxung area, southern Tibet. J. Asian Earth Sci. 33 (5–6), 323–336.

Rogers, J.J.W., Santosh, M., 2002. Configuration of Columbia, a Mesoproterozoic Supercontinent. Gondwana Res. 5 (1), 5–22.

Rollinson, H., 1993. Using Geochemical Data: Evaluation, Pre-sentation, Interpretation. Longman, London. 215–263 pp.

Rubatto, D., Hermann, J., Berger, A., Engi, M., 2009. Protracted fluid-induced melting during barrovian metamorphism in the central Alps. Contrib. Mineral. Petrol. 158 (6), 703–722.

Rubatto, D., 2017. Zircon: The Metamorphic Mineral. Rev. Mineral. Geochem. 83, 261–296.

Sadowski, G.R., Bettencourt, J.S., 1996. Mesoproterozoic tectonic correlations between eastern Laurentia and the western border of the Amazon Craton. Precambrian Res. 76 (3–4), 213–227.

Sawyer, E.W., 2001. Melt segregation in the continental crust: Distribution and movement of melt in anatectic rocks. J. Metamorph. Geol. 19 (3), 291–309.

Sengör, A.M.C., Natal'in, B.A., 1996. Paleotectonics of Asia: Fragments of a synthesis. In: Yin, A., Harrison, M.T. (Eds.), The Tectonic Evolution of Asia, Cambridge University Press, pp. 486–640.

Silveira, E.M., Söderlund, U., Oliveira, E.P., Ernst, R.E., Menezes Leal, A.B., 2013. First precise U–Pb baddeleyite ages of 1500 Ma mafic dykes from the São Francisco Craton, Brazil, and tectonic implications. Lithos 174, 144–156.

Sun, S.S., McDonough, W.F., 1989. Chemical and isotope systematics of oceanic basalts: Implications for mantle composition and processes. In: Saunders, A.D. (Ed.), Magmatism in Ocean Basins. Geological Society of London Special Publication, pp. 313–345.

Timmermann, H., Jamieson, R.A., Parrish, R.R., Culshaw, N.G., 2002. Coeval migmatitues and granulites, Muskoka domain, southwestern Grenville Province, Ontano. Can. J. Earth Sci. 39 (2), 239–258.

Veevers, J.J., 2004. Gondwanaland from 650–500 Ma assembly through 320 Ma merger in Pangea to 185–100 Ma breakup: Supercontinental tectonics via stratigraphy and radiometric dating. Earth Sci. Rev. 68, 1–132

Weis, D., 1986. Genetic implications of Pb isotopic geochemistry in the Rogaland anorthositic complex (southwest Norway). Chem. Geol. 57 (1), 181–199.

Weller, O.M., St-Onge, M.R., Searle, M.P., Waters, D.J., Rayner, N., Chen, S., Chung, S.L., Palin, R.M., 2015. Quantifying the *P–T–t* conditions of north–south Lhasa terrane accretion: New insight into the pre-Himalayan architecture of the Tibetan plateau. J. Metamorph. Geol. 33 (1), 91–113.

Xie, C.M., Li, C., Su, L., Wu, Y.W., Wang, M., Yu, H., 2010. LA–ICP–MS U–Pb dating of zircon from granite–gneiss in the Amdo area, northern Tibert, China. Geolo. Bull. Chin. 29 (12), 1737–1744 (in Chinese with English abstract).

Xie, R.W., Peng, X.J., Xiluelangjie, Bao, J.Y., Duan, G.X., He, C.H., Qiangbazhax, Sha, S.L., Chen, Y.M., Chen, D.Q., Peng, D.P., 2007. 1:250, 000 geological report of Zêtang Town with geological map. Geological Survey of Tibet

Autonomous Region Press, Lhasa, pp. 1–315 (in Chinese).

Xu, R.H., Schärer, U., Allègre, C.J., 1985. Magmatism and metamorphism in the Lhasa block (Tibet): A geochronological study. J. Geol. 93(1), 41–57.

Xu, W.C., Zhang, H.F., Harris, N., Guo, L., Pan, F.B., Wang, S., 2013a. Geochronology and geochemistry of Mesoproterozoic granitoids in the Lhasa terrane, south Tibet: Implications for the early evolution of Lhasa terrane. Precambrian Res. 236, 46–58.

Xu, W.C., Zhang, H.F., Harris, N., Guo, L., Pan, F.B., 2013b. Rapid Eocene erosion, sedimentation and burial in the eastern Himalayan syntaxis and its geodynamic significance. Gondwana Res. 23 (2), 715–725.

Yang, J.S., Xu, Z.Q., Li, Z.L., Xu, X.Z., Li, T.F., Ren, Y.F., Li, H.Q., Chen, S.Y., Robinson, P.T., 2009. Discovery of an eclogite belt in the Lhasa block, Tibet: A new border for Paleo-Tethys? J. Asian Earth Sci. 34 (1), 76–89.

Yang, Z.M., Hou, Z.Q., Jiang, Y.F., Zhang, H.R., Song, Y.C., 2011. Sr-Nd-Pb and zircon Hf isotopic constraints on petrogenesis of the Late Jurassic granitic porphyry at Qulong, Tibet. Acta Petrol. Sin. 27 (7), 2003–2010 (in Chinese with English abstract).

Yin, A., Harrison, T.M., 2000. Geologic evolution of the Himalayan–Tibetan orogen. Annu. Rev. Earth Planet. Sci. 28, 211–280.

Yin, A., Nie, S., 1996. A Phanerozoic palinspastic reconstruction of China and its neighboring regions. In: Yin, A., Harrison, M.T. (Eds.), The Tectonic Evolution of Asia. Cambridge University Press, pp. 442–485.

Yin, G.G., Chen, Y.P., Su, X.J., Bao, J.Y., Hou, S.Y., Lu, Y., Duan, G.X., Zhang, J.Y., Liu, Z., Xiao, L., 2003. 1:250,000 geological report of Nyingtri region with geological map. Yunnan, Institute of Yunnan Geological Survey (in Chinese).

Zeng, L.S., Liu, J., Gao, L.E., Chen, F.Y., Xie, K.J., 2009. Early Mesozoic high-pressure metamorphism within the Lhasa block, Tibet and implications for regional tectonics. Earth Sci. Front. 16 (2), 140–151.

Zeng, Y.C., Chen, Q, Xu, J.F., Chen, J.L., Huang, F., Yu, H.X., Zhao, P.P., 2018. Petrogenesis and geodynamic significance of neoproterozoic (~ 925 Ma) high-Fe-Ti gabbros of the Rentso ophiolite, Lhasa terrane, central Tibet. Precambrian Res. 314, 160–169.

Zhang, H.F., Xu, W.C., Guo, J.Q., Zong, K.Q., Cai, H.M., Yuan, H.L., 2007a. Zircon U–Pb and Hf isotopic composition of deformed granite in the southern margin of the Gangdese Belt, Tibet: Evidence for early Jurassic subduction of Neo-Tethyan oceanic slab. Acta Petrol. Sin. 23 (6), 1347–1353 (in Chinese with English abstract).

Zhang, H.F., Xu, W.C., Guo, J.Q., Zong, K.Q., Cai, H.M., Yuan, H.L., 2007b. Indosinian orogenesis of the Gangdese terrane: Evidences from zircon U–Pb dating and petrogenesis of granitoids. Earth Sci. J. China Univ. Geosci. 32 (2), 155–166 (in Chinese with English abstract).

Zhang, K.J., Zhang, Y.X., Li, B., Zhong, L.F., 2007. Nd isotopes of siliciclastic rocks from Tibet, western China: Constraints on provenance and pre-Cenozoic tectonic evolution. Earth Planet. Sci. Lett. 256 (3–4), 604–616.

Zhang, X.R., Shi, R.D., Huang, Q.S., Liu, D.L., Gong, X.H., Chen, S.S., Wu, K., Yi, G.D., Sun, Y.L., Ding, L., 2014. Early Jurassic high-pressure metamorphism of the Amdo terrane, Tibet: Constraints from zircon U-Pb geochronology of mafic granulites. Gondwana Res. 26 (3–4), 975–985.

Zhang, Z.M., Zhao, G.C., Santosh, M., Wang, J.L., Dong, X., Liou, J.G., 2010. Two stages of granulite facies metamorphism in the eastern Himalayan syntaxis, south Tibet: Petrology, zircon geochronology and implications for the subduction of Neo-Tethys and the Indian continent beneath Asia. J. Metamorph. Geol. 28 (7), 719–733.

Zhang, Z.M., Dong, X., Liu, F., Lin, Y.H., Yan, R., Santosh, M., 2012a. Tectonic evolution of the Amdo terrane, central Tibet: Petrochemistry and zircon U–Pb geochronology. J. Geol. 120 (4), 431–451.

Zhang, Z.M., Dong, X., Liu, F., Lin, Y.H., Yan, R., He, Z.Y., Santosh, M., 2012b. The making of Gondwana: Discovery of 650 Ma HP granulites from the North Lhasa, Tibet. Precambrian Res. 212–213, 107–116.

Zhang, Z.M., Dong, X., Xiang, H., Liou, J.G., Santosh, M., 2013. Building of the deep Gangdese arc, South Tibet: Paleocene plutonism and granulite-facies metamorphism. J. Petrol. 54 (12), 2547–2580.

Zhang, Z.M., Dong, X., Santosh, M., Zhao, G.C., 2014a. Metamorphism and tectonic evolution of the Lhasa terrane, Central Tibet. Gondwana Res. 25 (1), 170–189.

Zhang, Z.M., Dong, X., Xiang, H., He, Z.Y., Liou, J.G., 2014b. Metagabbros of the Gangdese arc root, south Tibet: Implications for the growth of continental crust

Geochim. Cosmochim. Acta 143, 268–284.

Zhang, Z.M., Dong, X., Xiang, H., Ding, H.X., He, Z.Y., Liou, J.G., 2015. Reworking of the Gangdese magmatic arc, southeastern Tibet: Post-collisional metamorphism and anatexis. J. Metamorph. Geol. 33 (1), 1–21.

Zhao, G.C., Sun, M., Wilde, S.A., Li, S.Z., 2003. Assembly, accretion, and break-up of the Palaeo-Mesoproterozoic Columbia supercontinent: Record in the North China Craton revisited. Gondwana Res. 6 (3), 417–434.

Zhu, D.C., Pan, G.T., Chung, S.L., Liao, Z.L., Wang, L.Q., Li, G.M., 2008. SHRIMP zircon age and geochemical constraints on the origin of lower Jurassic volcanic rocks from the Yeba formation, southern Gangdese, south Tibet. Int. Geol. Rev. 50 (5), 442–471.

Zhu, D.C., Mo, X.X., Niu, Y., Zhao, Z.D., Wang, L.Q., Liu, Y.S., Wu, F.Y., 2009a. Geochemical investigation of Early Cretaceous igneous rocks along an east–west traverse throughout the central Lhasa Terrane, Tibet. Chem. Geol. 268 (3–4), 298–312.

Zhu, D.C., Mo, X.X., Niu, Y.L., Zhao, Z.D., Wang, L.Q., Pan, G.T., Wu, F.Y., 2009b. Zircon U–Pb dating and in-situ Hf isotopic analysis of Permian peraluminous granite in the Lhasa terrane, southern Tibet: Implications for Permian collisional orogeny and paleogeography. Tectonophysics 469 (1–4), 48–60.

Zhu, D.C., Zhao, Z.D., Niu, Y.L., Mo, X.X., Chung, S.L., Hou, Z.Q., Wang, L.Q., Wu, F.Y., 2011. The Lhasa Terrane: Record of a microcontinent and its histories of drift and growth. Earth Planet. Sci. Lett. 301 (1–2), 241–255.

Zhu, D.C., Zhao, Z.D., Niu, Y.L., Dilek, Y., Wang, Q., Ji, W.H., Dong, G.C., Sui, Q.L., Liu, Y.S., Yuan, H.L., Mo, X.X., 2012. Cambrian bimodal volcanism in the Lhasa Terrane, southern Tibet: Record of an early Paleozoic Andean-type magmatic arc in the Australian proto-Tethyan margin. Chem. Geol. 328, 290–308.

Zhu, D.C., Zhao, Z.D., Niu, Y., Dilek, Y., Hou, Z.Q., Mo, X.X., 2013. The origin and pre-Cenozoic evolution of the tibetan plateau. Gondwana Res. 23 (4), 1429–1454.

Figure captions:

Figure 1. (a) Tectonic framework of the Tibetan Plateau (after Zhu et al., 2013), showing the major tectonic subdivisions. NLT = Northern Lhasa subterrane, CLT = Central Lhasa subterrane, SLT = Southern Lhasa subterrane, JSSZ = Jinsha Suture Zone, LSSZ = Longmu Tso-Shuanghu Suture Zone, BNSZ = Bangong-Nujiang Suture Zone, SNMZ = Shiquan River-Nam Tso Mélange Zone, LMF = Luobadui-Milashan Fault, IYZSZ = Indus-Yarlung Zangbo Suture Zone. Data sources of the Precambrian magmatic rocks for Amdo: ~ 820 Ma and 500 Ma (Zhang et al., 2012a), 852 Ma (Guynn et al., 2006), 532 Ma (Guynn et al., 2012); the CLT from west to east: 492 Ma (Zhu et al., 2012), 525–510 Ma (Hu et al., 2013), 512 Ma (Ding et al., 2015), 787 Ma (Hu et al., 2005), 897–886 Ma (Zhang et al., 2012b), 760 Ma (Hu et al., 2018a), 822–806 Ma (Hu et al., 2018b), 925 Ma (Zeng et al., 2018), 1343–1250 Ma

(Xu et al., 2013a; Chen et al., 2019), 1866 Ma (Chen et al., 2019); the SLT: 496 Ma (Dong et al., 2010). (b) Geological sketch map of the Dongjiu area in the SLT, the Paleoproterozoic data (~ 1780 Ma) from Lin et al. (2013b).

Figure 2. Photomicrographs of representative Dongjiu gneiss. (a) Biotite (Bt)-amphibole (Amp) gneiss, consisting of amphibole, plagioclase (Pl), K-feldspar (Kfs), biotite, quartz (Qz) and titanite (Ttn) riming ilmenite (Ilm), with minor apatite (Ap). (b) Bt-amp gneiss, showing plagioclase with cuspate extensions along quartz-quartz contacts. (c) and (d) Bt-amp gneiss, showing allanite (Aln) replaced by epidote (Ep) in rim, with zircon (Zrn) inclusions. (e) Bt gneiss, consisting of plagioclase, K-feldspar, biotite, quartz, with minor allanite replaced by epidote at rim; adjacent grains of quartz, plagioclase and K-feldspar are corroded. (f) Bt gneiss, showing adjacent plagioclase and biotite grains are corroded; narrow K-feldspar blebs at quartz-plagioclase contacts.

Figure 3. (a) Ab-An-Or classification for silicic rocks from Barker (1979). (b) A/CNK vs A/NK diagram from Maniar and Piccoli (1989). The data of the Bomi Mesoproterozoic granitoids are after Xu et al. (2013a).

Figure 4. (a) Chondrite-normalized REE and (b) Primitive-mantle-normalized trace element patterns for the Dongjiu gneiss. The data of the Bomi Mesoproterozoic granitoids are after Xu et al. (2013a). The normalization data are from Sun and

McDonough (1989).

Figure 5. Zircon U–Pb concordia diagrams and chondrite-normalized REE patterns of the Dongjiu Bt-amp gneiss. (a), (c) and (e) Zircon U–Pb concordia diagrams, red and blue elliptises represent zircon core and rim ages, respectively. (b), (d) and (f) Chondrite-normalized REE patterns, showing CL images of representative zircon grains. Red and blue circles indicate zircon core and rim dating spots with ages in Ma, respectively. The normalization data are from Sun and McDonough (1989).

Figure 6. Zircon U–Pb concordia diagrams and chondrite-normalized REE patterns of the Dongjiu Bt gneiss. (a) and (c) Zircon U–Pb concordia diagrams, red and blue ellipses represent zircon core and rim ages, respectively. (b) and (d) Chondrite-normalized REE patterns, showing CL images of representative zircon grains. Red and blue circles indicate zircon core and rim ages with ages in Ma, respectively. The normalization data are from Sun and McDonough (1989).

Figure 7. BSE images and photomicrographs of representative titanite for the Dongjiu Bt-amp gneiss. Representative titanite (a)–(h) for sample 169-1, (i)–(p) for sample 39-1. (a)–(d) and (i)–(l) Blue circles are spots for dating with ^{207}Pb corrected $^{206}Pb/^{238}U$ ages in Ma. (e)–(h) and (m)–(p) Most titanite including ilmenite, biotite, allanite, apatite, plagioclase, quartz and minor rutile.

Figure 8. Titanite U–Pb concordia diagrams of the Dongjiu Bt-amp gneiss.

Figure 9. Frequency histogram of Zr-in-titanite temperatures for the Dongjiu Bt-amp gneiss.

Figure 10. Zircon U vs Th contents diagram of the Dongjiu gneiss.

Figure 11. Zircon U-Pb age vs $\varepsilon_{Hf}(t)$ diagram for the Dongjiu gneiss and related rocks from the Lhasa terrane. Data sources: SLT ~ 1500 Ma gneiss (our unpublished data); SLT granitoids (Chu et al., 2006; Zhang et al., 2007a; Ji et al., 2009, 2012; Yang et al., 2011; Zhu et al. 2011; Dong et al., 2013, 2014, 2015; Guo et al., 2013; Meng et al., 2016); CLT granitoids (Zhang et al., 2007b; Zhu et al., 2009b, 2011, 2012; Xu et al., 2013a; Hu et al., 2018b; Chen et al., 2019); SLT Paleozoic strata (Guo et al., 2017); CLT Paleozoic strata (Zhu et al., 2013; Li et al., 2014).

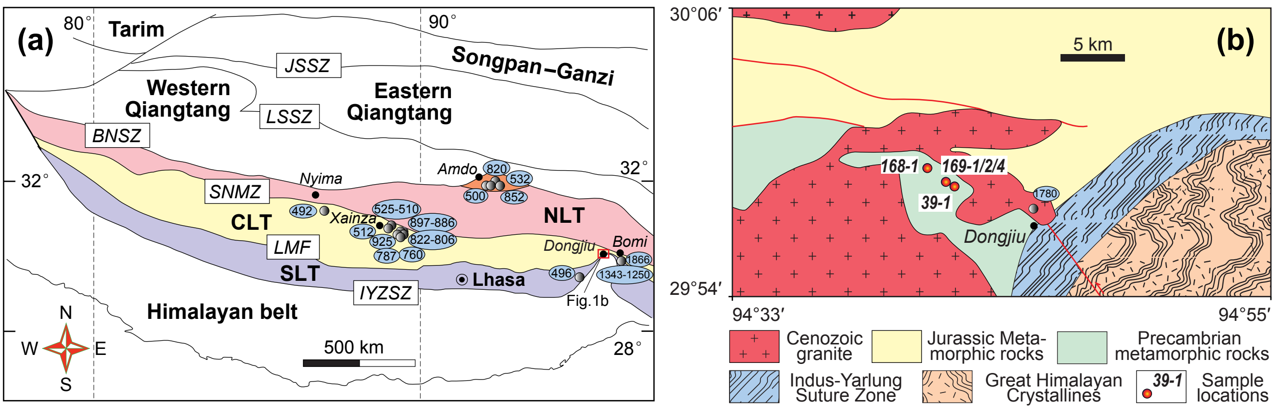

Figure 1
(a) Tectonic framework of the Tibetan Plateau, showing the major tectonic subdivisions. NLT = Northern Lhasa subterrane, CLT = Central Lhasa subterrane, SLT = Southern Lhasa subterrane, JSSZ = Jinsha Suture Zone, LSSZ = Longmu Tso-Shuanghu Suture Zone, BNSZ = Bangong-Nujiang Suture Zone, SNMZ = Shiquan River-Nam Tso Mélange Zone, LMF = Luobadui-Milashan Fault, IYZSZ = Indus-Yarlung Zangbo Suture Zone.
(b) Geological sketch map of the Dongjiu area in the SLT.

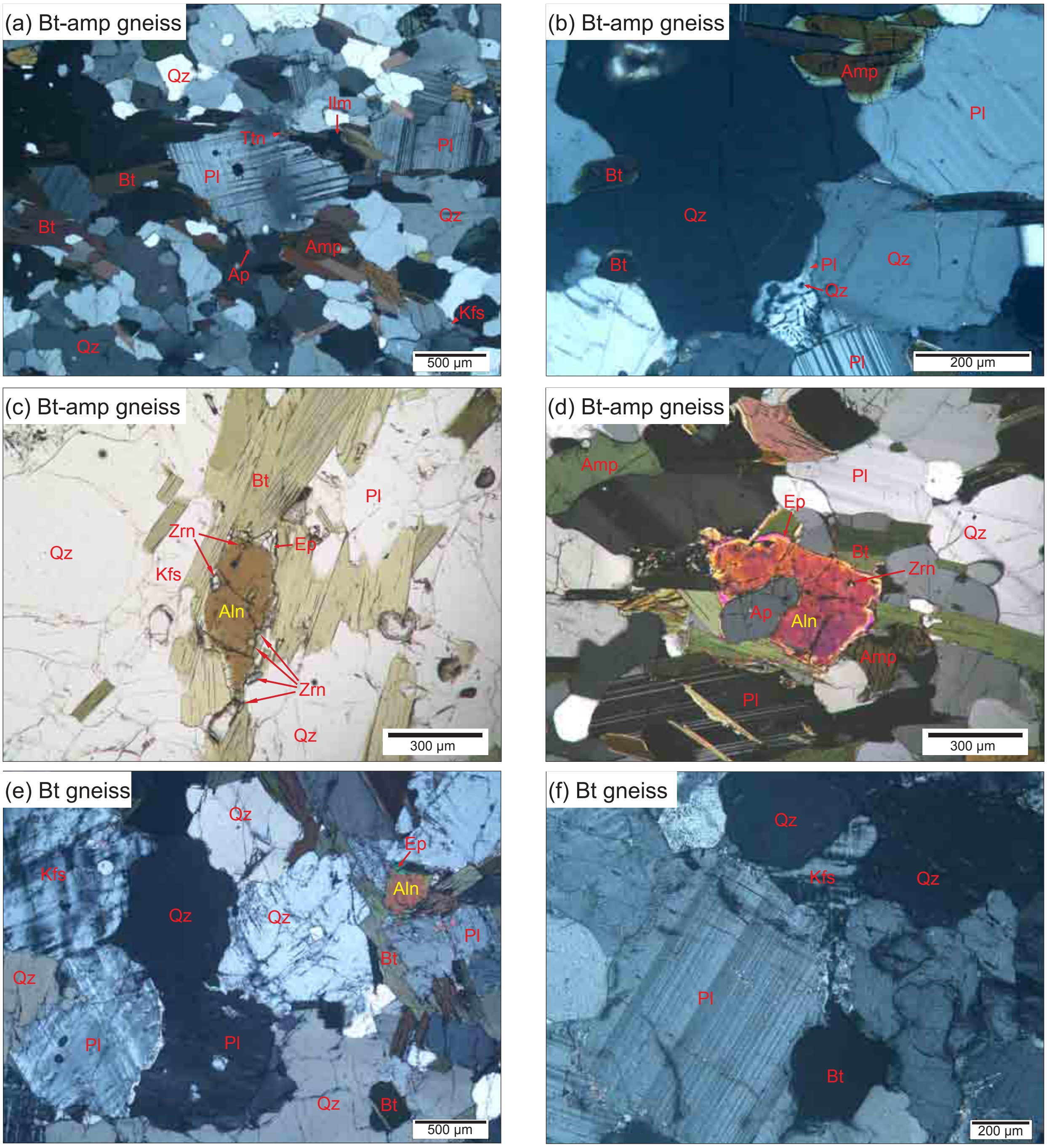

Figure 2. Photomicrographs of representative Dongjiu gneiss.
(a) Biotite (Bt)- amphibole (amp) gneiss, consisting of amphibole, plagioclase (Pl), K-feldspar (Kfs), biotite, quartz (Qz) and titanite (Ttn) riming ilmenite (Ilm), with minor apatite (Ap).
(b) Bt-amp gneiss, showing plagioclase with cuspate extensions along quartz-quartz contacts.
(c) and (d) Bt-amp gneiss, showing allanite (Aln) replaced by epidote (Ep) in rim, with zircon (Zrn) inclusions.
(e) Bt gneiss, consisting of plagioclase, K-feldspar, biotite, quartz, with minor allanite replaced by epidote at rim; adjacent quartz, plagioclase and K-feldspar grains are corroded.
(f) Bt gneiss, showing adjacent plagioclase and biotite grains are corroded; narrow K-feldspar blebs at quartz-plagioclase contacts.

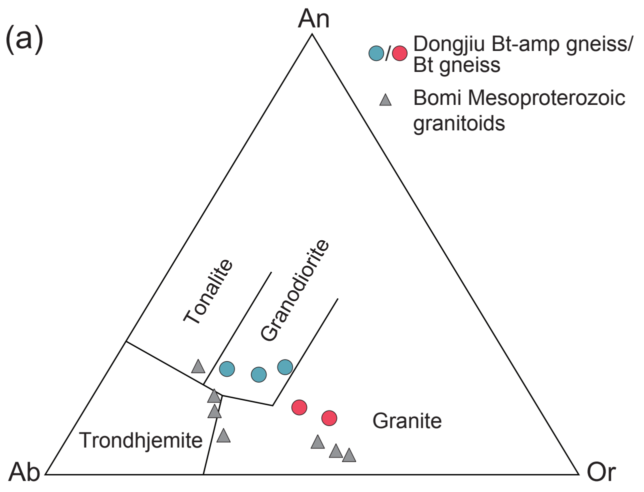

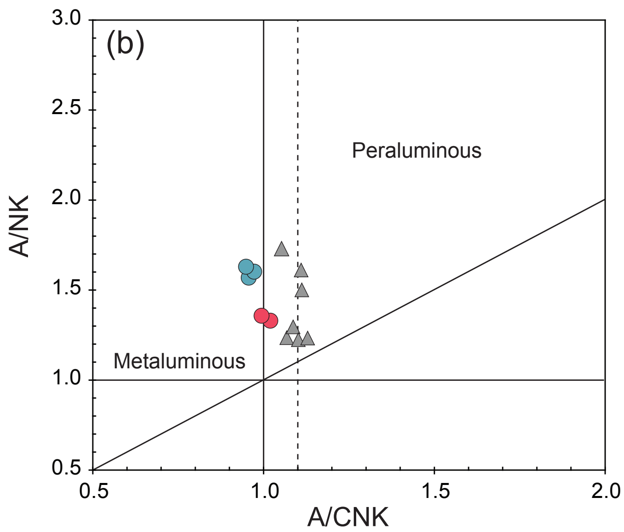

Figure 3
(a) Ab-An-Or classification for silicic rocks.
(b) A/CNK vs A/NK diagram.

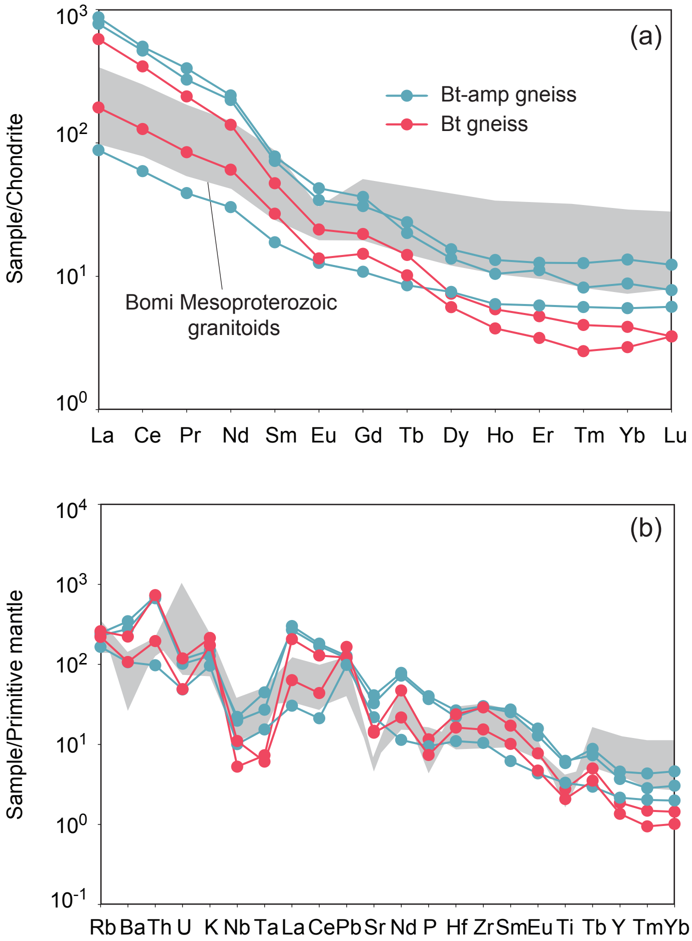

Figure 4
(a) Chondrite-normalized REE.
(b) Primitive-mantle-normalized trace element patterns for the Dongjiu gneiss.

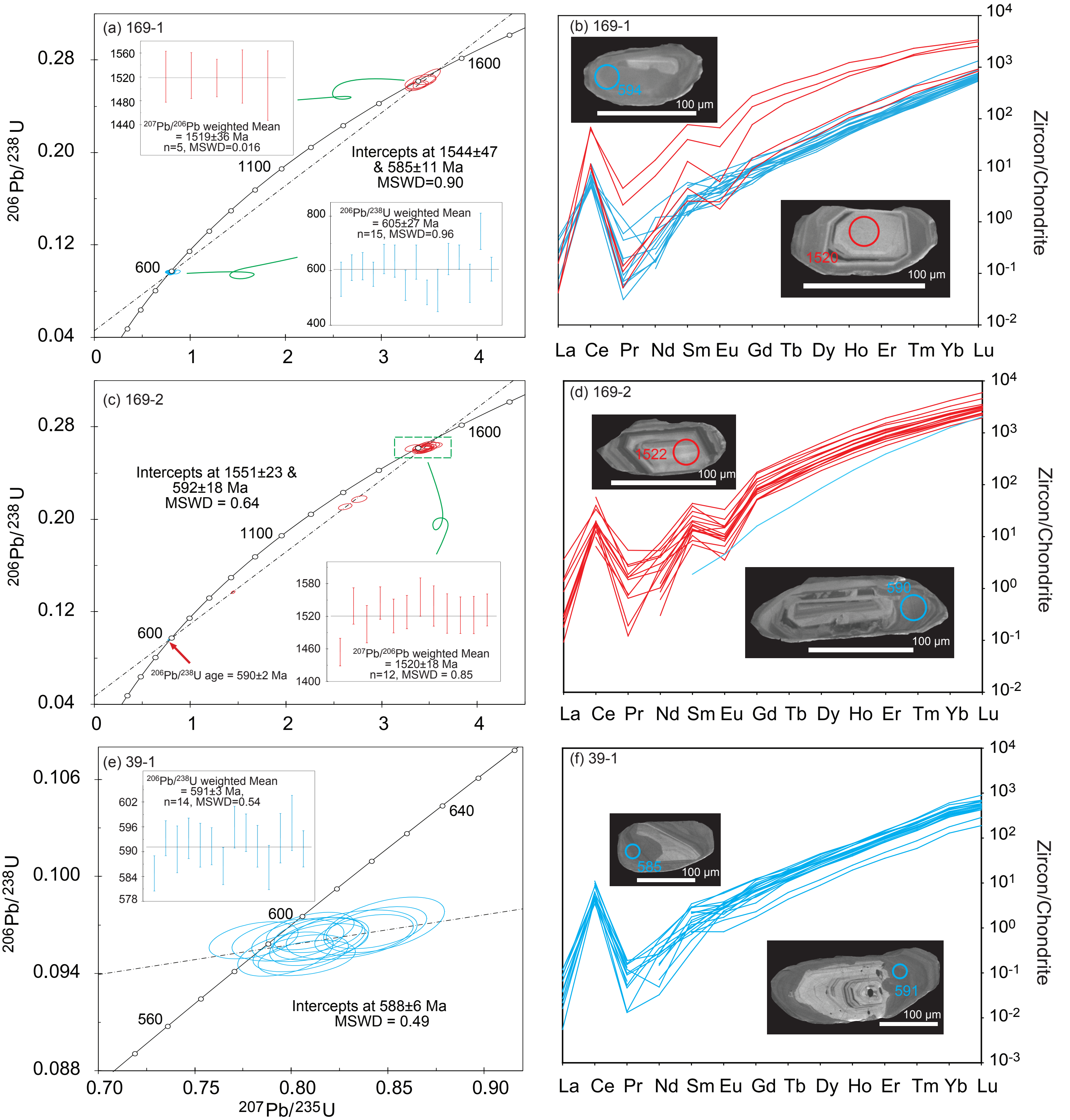

Figure 5. Zircon U–Pb concordia diagrams and chondrite-normalized REE patterns of the Dongjiu Bt-amp gneiss.

(a), (c) and (e) Zircon U–Pb concordia diagrams, red and blue elliptises represent zircon core and rim ages, respectively.

(b), (d) and (f) Chondrite-normalized REE patterns, showing CL images of representative zircon grains. Red and blue circles indicate zircon core and rim dating spots with ages in Ma, respectively.

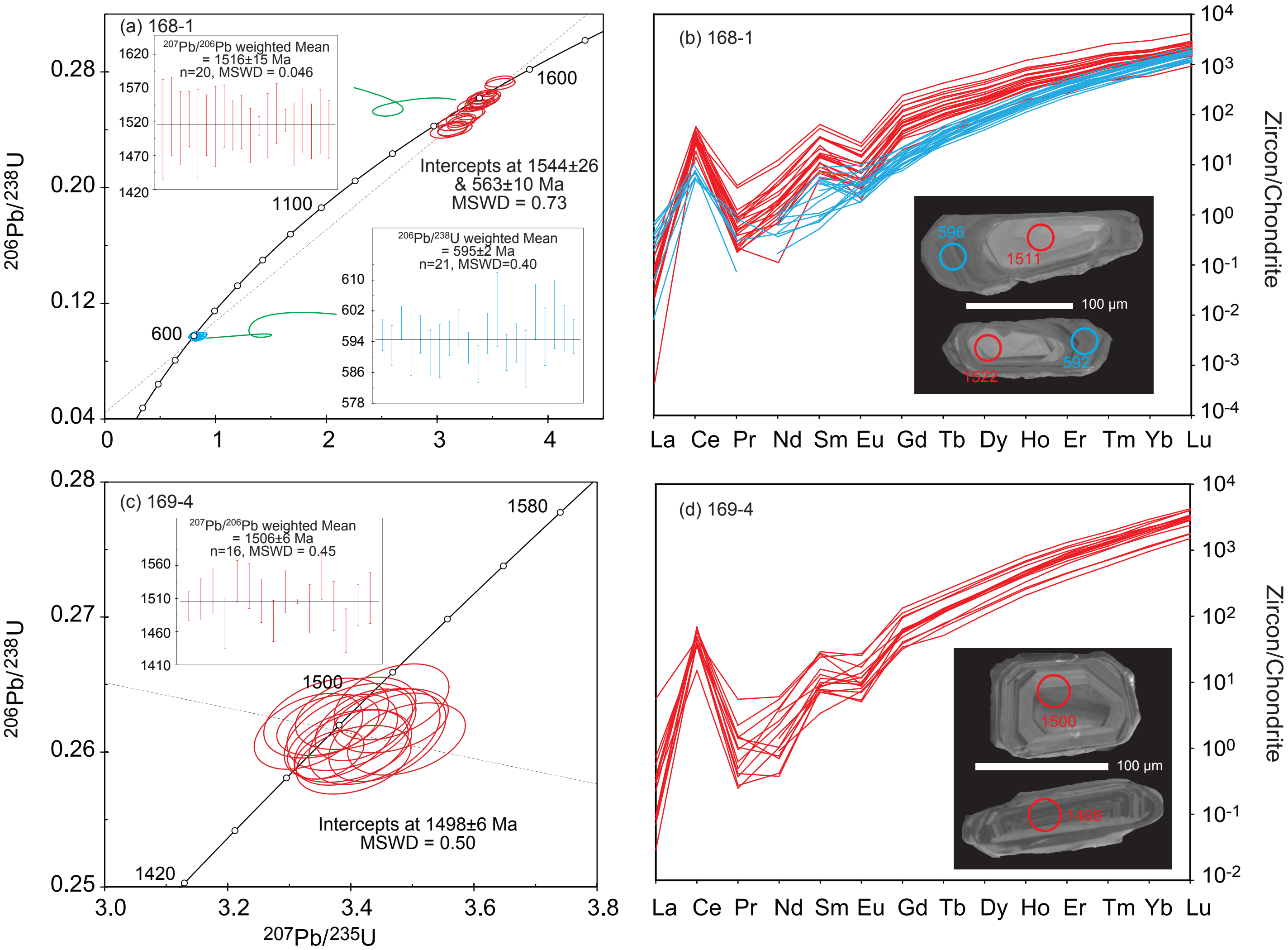

Figure 6. Zircon U–Pb concordia diagrams and chondrite-normalized REE patterns of the Dongjiu Bt gneiss.

(a) and (c) Zircon U–Pb concordia diagrams, red and blue ellipses represent zircon core and rim ages, respectively.
(b) and (d) Chondrite-normalized REE patterns, showing CL images of representative zircon grains. Red and blue circles indicate zircon core and rim ages with ages in Ma, respectively.

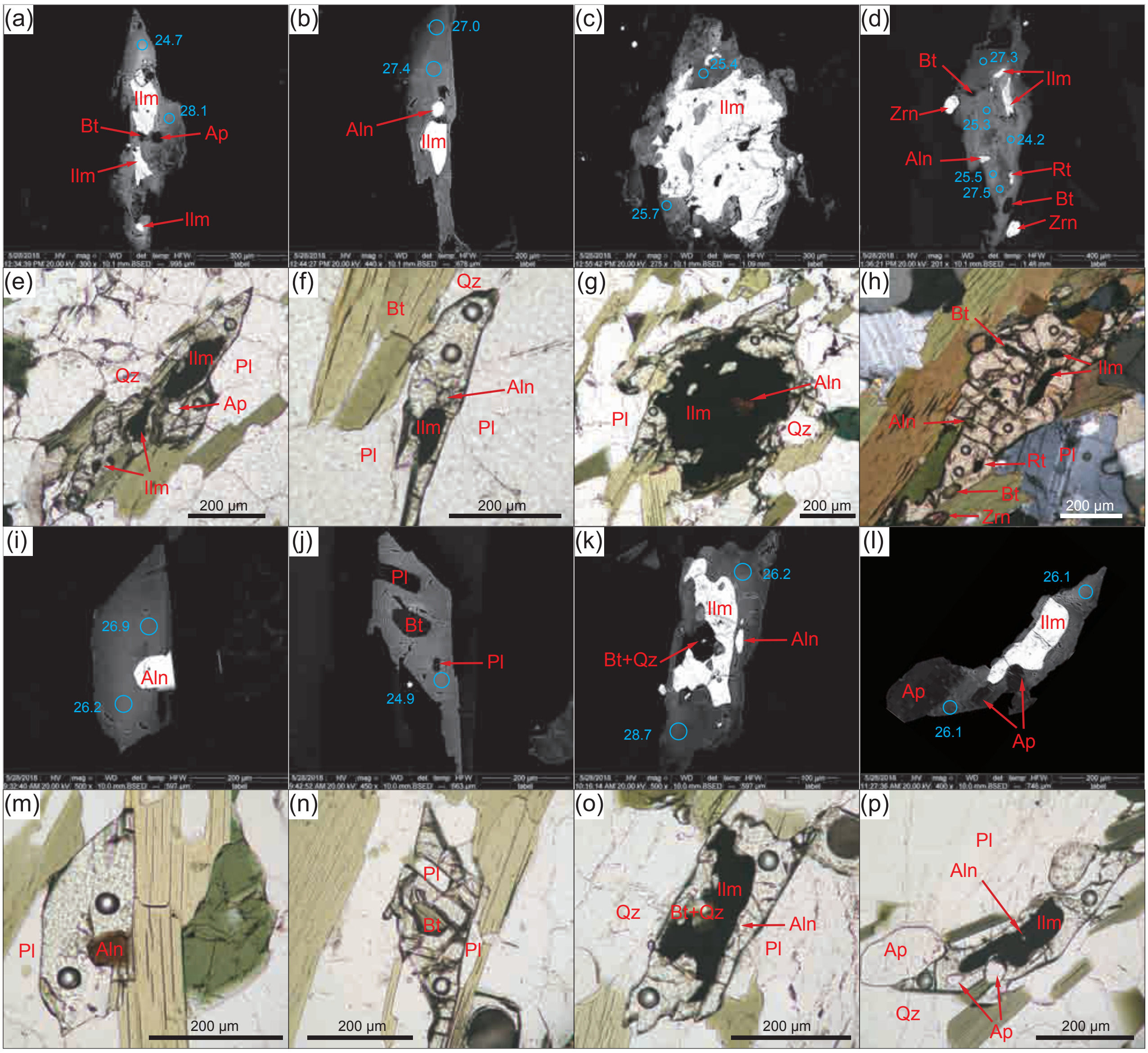

Figure 7. BSE images and photomicrographs of representative titanite for the Dongjiu Bt-amp gneiss.

Representative titanite (a)–(h) for sample 169-1, (i)–(p) for sample 39-1. (a)–(d) and (i)–(l) Blue circles are spots for dating with ^{207}Pb corrected ^{206}Pb/^{238}U ages in Ma. (e)–(h) and (m)–(p) Most titanite including ilmenite, biotite, allanite, apatite, plagioclase, quartz and minor rutile.

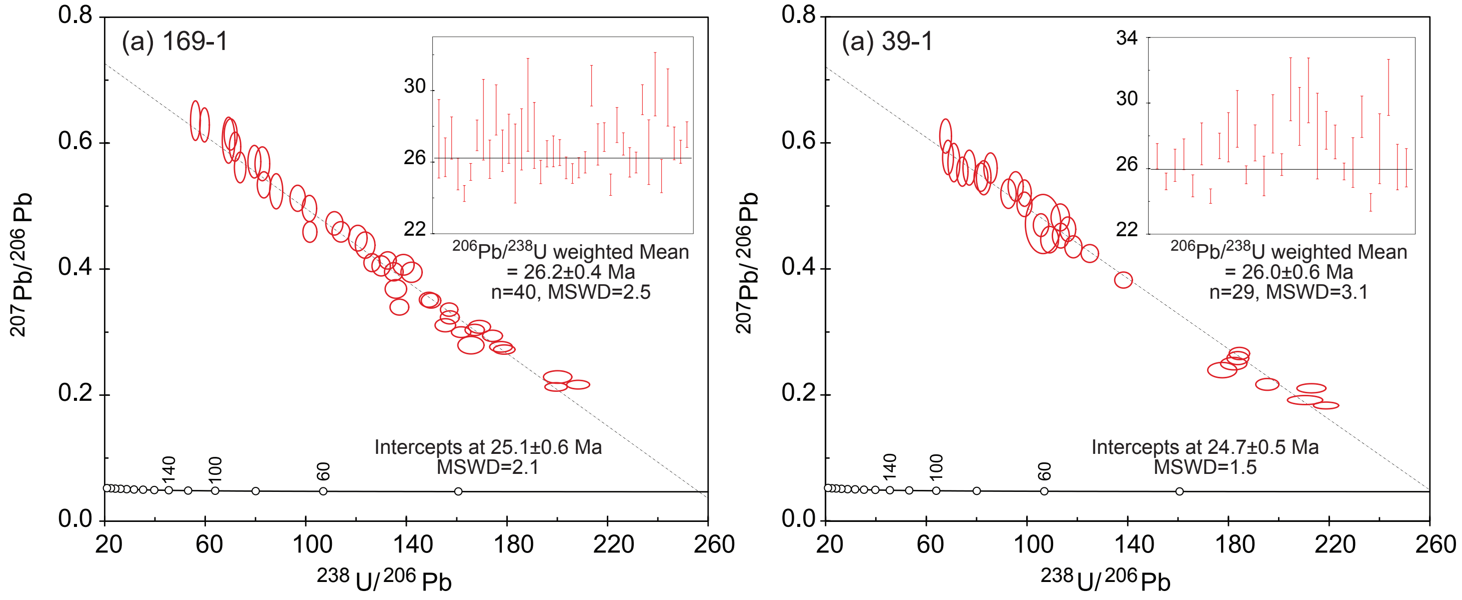

Figure 8. Titanite U–Pb concordia diagrams of the Dongjiu Bt-amp gneiss.

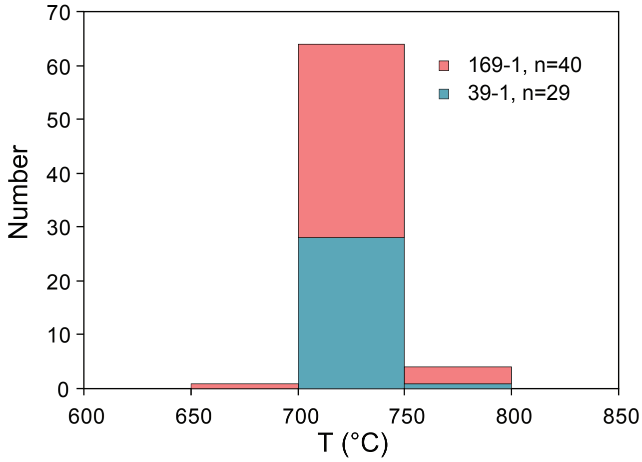

Figure 9. Frequency histogram of Zr-in-titanite temperatures for the Dongjiu Bt-amp gneiss

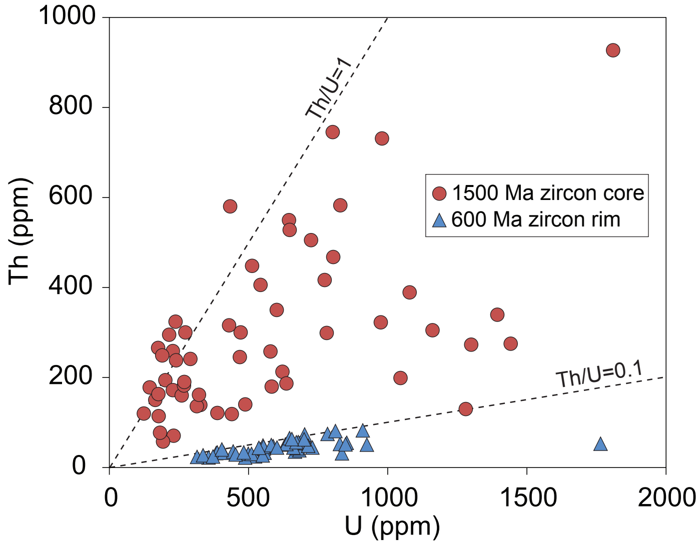

Figure 10. Zircon U vs Th contents diagram of the Dongjiu gneiss

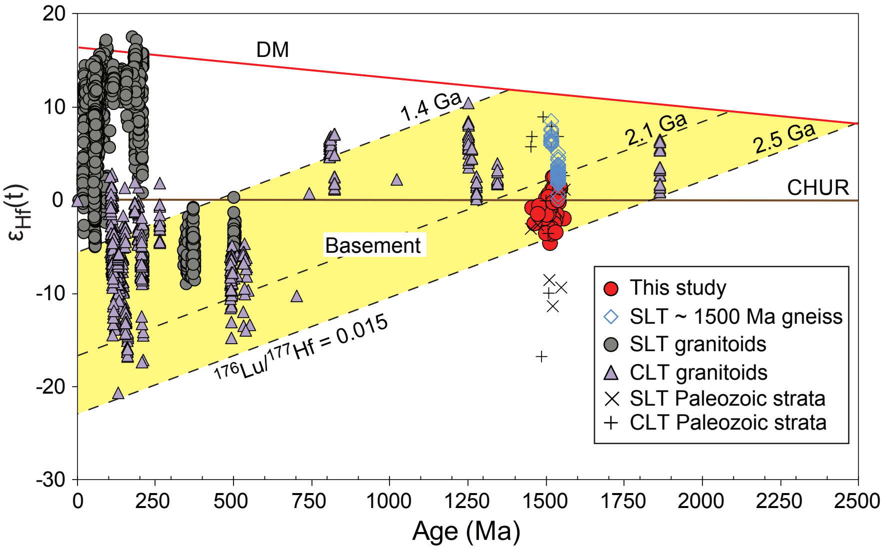

Figure 11. Zircon U-Pb age vs $\varepsilon_{Hf}(t)$ diagram for the Dongjiu gneiss and related rocks from the Lhasa terrane

CONFICT OF INTEREST

Xin Dong and all co-authors confirm that there are no known conflicts of interest associated with this publication (Title: Reworked Precambrian metamorphic basement of the Lhasa terrane, southern Tibet: Zircon/Titanite U–Pb geochronology, Hf isotope and Geochemistry) and there has been no significant financial support for this work that could have influenced its outcome.